NPS-67-86-005CR

NAVAL POSTGRADUATE SCHOOL
Monterey, California

CONTRACTOR REPORT

VISCOUS-INVISCID INTERACTION ANALYSIS OF INCOMPRESSIBLE CASCADE FLOWS

ANDREAS KRAINER

December 1986

Prepared for: Naval Air Systems Command
Code Air 931E

NAVAL POSTGRADUATE SCHOOL
MONTEREY, CALIFORNIA 93943-5100

Rear Admiral R. C. Austin
Superintendent

D. A. Schrady
Provost

The work reported herein was performed for the Naval Postgraduate School by Mr. A. Krainer under contract number N62271-85-M-0437. This work is in support of "Investigation of Turbomachinery Cascade Flows" sponsored by the Naval Air Systems Command, Code 931E. The report provides information concerning the use of viscous-inviscid interaction methods to predict incompressible cascade flows. The project at the Naval Postgraduate School is under the cognizance of Professor M. F. Platzer who is the principal investigator.

ECRITY CLASSIFICATION OF THIS PAGE

REPORT DOCUMENTATION PAGE

a. EPORT SECURITY CLASSIFICATION /NCLASSIFIED	1b. RESTRICTIVE MARKINGS NONE
a. ECURITY CLASSIFICATION AUTHORITY	3. DISTRIBUTION / AVAILABILITY OF REPORT Approved for public release; distribution is unlimited
b. ECLASSIFICATION / DOWNGRADING SCHEDULE	
RFORMING ORGANIZATION REPORT NUMBER(S) PS-67-86-005CR	5. MONITORING ORGANIZATION REPORT NUMBER(S) NPS-67-86-005CR
AME OF PERFORMING ORGANIZATION ANDREAS KRAINER	6b. OFFICE SYMBOL (*If applicable*) Code 67
	7a. NAME OF MONITORING ORGANIZATION Naval Postgraduate School
DDRESS (*City, State, and ZIP Code*) Naval Postgraduate School Department of Aeronautics Monterey, CA 93943-5100	7b. ADDRESS (*City, State, and ZIP Code*) Naval Postgraduate School Department of Aeronautics Monterey, CA 93943-5100
AME OF FUNDING / SPONSORING RGANIZATION Naval Air Systems Command	8b. OFFICE SYMBOL (*If applicable*) Air 931E
	9. PROCUREMENT INSTRUMENT IDENTIFICATION NUMBER
DDRESS (*City, State, and ZIP Code*)	10. SOURCE OF FUNDING NUMBERS

PROGRAM ELEMENT NO.	PROJECT NO.	TASK NO.	WORK UNIT ACCESSION NO.

ITLE (*Include Security Classification*)

ISCOUS-INVISCID INTERACTION ANALYSIS OF INCOMPRESSIBLE CASCADE FLOWS (UNCLASSIFIED)

ERSONAL AUTHOR(S) Andreas Krainer

TYPE OF REPORT	13b. TIME COVERED	14. DATE OF REPORT (*Year, Month, Day*)	15. PAGE COUNT
Annual	FROM Sep 85 TO Aug 86	December 1986	48

UPPLEMENTARY NOTATION

COSATI CODES			18. SUBJECT TERMS (*Continue on reverse if necessary and identify by block number*)
FIELD	GROUP	SUB-GROUP	Incompressible cascade aerodynamics Boundary layer flows Viscous-inviscid interaction

BSTRACT (*Continue on reverse if necessary and identify by block number*)

aerodynamic performance of turbomachines is limited by flutter, choking, and stall, the last of which being a topic of this rt. Viscous flow considerations are not only essential in determining loss coefficients, but also in ascertaining loadings and roviding a fundamental understanding of the flow. The focus of this report is on steady, incompressible, viscous, 2-d flows ugh a single infinite row of equidistant blades. In order to compute these cascade flows Prandtl's boundary layer concept anced by a strong interaction model is applied to the Navier-Stokes equations. Since this approach enables the integration oundary layer equations in the presence of backflow, it is an attractive alternative to more expensive Navier-Stokes solvers.

eci and collaborators, who developed such a viscous-inviscid interaction method for single airfoils, modified and extended r code to the cascade problem. The present contribution consists of a detailed description of the theory and of conducting a sample calculations. Flows past staggered cascades, using the ten percent thick airfoils of the NACA-65-series, were studied a range of Reynolds numbers and air inlet angles. Difficulties were encountered in cases of low Reynolds number and ly loaded blades. The apparent success of the single airfoil code and its close agreement with experiments could not yet be nded to the cascade problem, partly because of the more demanding airfoil shapes used in turbomachines and partly because ie inadequacy of the turbulence model at low Reynolds numbers. Improvements concerning both numerics and physics are ssary to turn the current cascade code into a robust and efficient tool to analyse cascade flows of practical interest.

DISTRIBUTION / AVAILABILITY OF ABSTRACT	21. ABSTRACT SECURITY CLASSIFICATION
☒ UNCLASSIFIED/UNLIMITED ☐ SAME AS RPT. ☐ DTIC USERS	UNCLASSIFIED
NAME OF RESPONSIBLE INDIVIDUAL Prof. Max F. Platzer	22b. TELEPHONE (*Include Area Code*) 408/646-2311
	22c. OFFICE SYMBOL Code 67Pl

FORM 1473, 84 MAR 83 APR edition may be used until exhausted. All other editions are obsolete

SECURITY CLASSIFICATION OF THIS PAGE

☆ U.S. Government Printing Office: 1986—606-24

VISCOUS-INVISCID INTERACTION ANALYSIS OF INCOMPRESSIBLE CASCADE FLOWS

By
ANDREAS KRAINER
Naval Postgraduate School,
Department of Aeronautics,
Monterey, CA 93943

ABSTRACT

The aerodynamic performance of turbomachines is limited by flutter, choking, and stall, the last of which being a topic of this report. Viscous flow considerations are not only essential in determining loss coefficients, but also in ascertaining loadings and in providing a fundamental understanding of the flow. However, because of the complexity of flows in turbomachines flow problems of model character only are accessible to numerical treatment. The focus of this report is on steady, incompressible, viscous, 2-d flows through a single infinite row of equidistant blades. In order to compute these cascade flows Prandtl's boundary layer concept enhanced by a strong interaction model is applied to the Navier-Stokes equations. Since this approach enables the integration of boundary layer equations in the presence of backflow, it is an attractive alternative to much more expensive Navier-Stokes solvers.

Cebeci and collaborators, who developed such a viscous-inviscid interaction method for single airfoils, modified and extended their code to the cascade problem. The present contribution consists of a detailed description of the theory and of conducting a few sample calculations of test-character. Flows past staggered cascades, using the ten percent thick airfoils of the NACA-65-series compressor blade family as cross sections, were studied over a range of Reynolds numbers and air inlet angles. Difficulties were encountered in cases of low Reynolds number and highly loaded blades. The apparent success of the single airfoil code and its close agreement with experiments could not yet be extended to the cascade problem, partly because of the more demanding airfoil shapes used in turbomachines and partly because of the inadequacy of the turbulence model at low Reynolds numbers. Improvements concerning both numerics and physics are necessary to turn the current cascade code into a robust and efficient tool to analyse cascade flows of practical interest.

TABLE OF CONTENTS

LIST OF FIGURES

LIST OF SYMBOLS

Latin symbols

A_{ij}, B_{ij}	Influence coefficients, representing normal and tangential velocities
b	$1 + \nu_t/\nu$
c	Chord length
c_f	Local skin friction coefficient
$c_{ik}, \tilde{c}_{ik}$	Interaction coefficients
C_L	Lift coefficient
F	Resultant gross force
f	Dimensionless streamfunction
h, k	Mesh sizes in η and x-direction
l_j	Length of j-th panel
m	Dimensionless pressure gradient parameter
n, t	Outer normal and clockwise tangential direction with respect to surface
R_c	Reynolds number based on reference velocity and chord length
R_x	Reynolds number based on external velocity and streamwise coordinate
R_θ	Reynolds number based on external velocity and momentum thickness
U, V	x and y-component of total velocity First and second η-derivative of dimensionless streamfunction
u, v	x and y-component of disturbance velocity x and y-velocity component in curvilinear system
u_e	External velocity
u_{eI}	Inviscid external velocity
$u_{e\delta}$	Correction term of inviscid external velocity due to viscous effects
u_0	Reference velocity
U_∞	Magnitude of vector mean velocity
$\vec{V}$	Total velocity vector
V_n, V_t	Normal and tangential component of total velocity
V_{wt}	Wall transpiration velocity
W	Dimensionless external velocity
x, y	Cartesian coordinates Curvilinear coordinates
x_i, y_i	Coordinates of i-th midpoint
X_j, Y_j	Coordinates of j-th panel boundary point

Greek symbols

α	Angle of vector mean velocity measured from axial direction
α_1, α_2	Air inlet and outlet angle, flow angles at up- and downstream infinity measured from axial direction
Γ	Circulation
γ	Stagger angle, angle between blade chord line and axial direction (counterclockwise positive) Vortex strength
γ_{tr}	Intermittency factor
δ	Boundary layer thickness
δ^*	Displacement thickness
η	Dimensionless normal coordinate
θ	Momentum thickness
θ_j	Angle between surface direction of j-th panel and positive x-axis
ν	Kinematic viscosity
ν_t	Eddy viscosity
ρ	Density of fluid
σ	Source strength
τ	Cascade spacing
Φ	Total velocity potential
φ	Disturbance velocity potential
ψ	Streamfunction
ω	Relaxation parameter

Sub- and superscripts

e	Boundary layer edge
i, j	Point where velocity is induced and location of singularity distribution that induces Grid point location
tr	Onset of transition
$1, 2, \ldots, N$	Panel numbering, starting at trailing edge, proceeding clockwise around blade, and ending even there
1, 2	Inlet and outlet plane
(0)	Basic flow at zero angle of attack
(90)	Basic flow at ninety degrees angle of attack
(γ)	Basic flow with circulation only
$'$	Differentiation with respect to η
∞	Uniform stream
κ	Number of Newton iterations

1. INTRODUCTION AND GENERAL CONCEPTS

Stall, the phenomenon at which lift decreases with an increase in angle of incidence, is one of the limiting factors in the efficient operation of turbomachines. The flow regime at stall is characterized by flow separation leading to regions of reversed flow, which do not only determine the loss behaviour but cause significant changes in loading and overall lift force. Flow separation is also present in another flow regime, i.e. bubble transition, which is a low Reynolds number flow phenomenon, comprising laminar separation, transition, and turbulent reattachment. Because of economical requirements on turbomachines, which result in higher blade loadings, the aerodynamic community is forced to provide a better understanding of viscous effects in both attached and separated flow. The increasing costs of wind tunnel experiments and the decreasing computing costs encourage the development of new numerical tools. Solutions of the full Navier-Stokes equations are still reserved for supercomputers, and on the other hand, classical boundary layer codes are restricted to attached flows. Therefore, engineers have developed procedures, which do the job of a Navier-Stokes solver at a lower expense of computing time and storage. Such procedures are based on the viscous-inviscid interaction concept which will be used in the present analysis.

What are the ingredients of a successful viscous-inviscid interaction method? Following Prandtl's boundary layer concept the computational domain is divided into an inviscid region and a thin layer, close to the blade's surface, where viscous effects cannot be neglected. The computational scheme solves separately for the flows in the viscous and inviscid domains, which was already a feature of classical boundary layer codes, but the essential point is the mechanism how inviscid and viscous flows are matched. While classical boundary layer methods suffer from a pronounced hierarchy of viscous and inviscid regions, interaction models are supposed to exhibit the ability of mutual and immediate transfer of information between viscous and inviscid regions. In summary, interaction methods must include an inviscid flow solution, a boundary layer method, able of handling both attached and separated flow, and some interaction model.

At this point we have to concede that our numerical possibilities are not even close to a solution of the flow inside a turbomachine. Unsteadiness, compressibility, highly 3-d character, interaction of shocks and wakes, and complex flow boundaries, as found in turbomachines, move a solution of the real problem far beyond today's potential. Because of the need to come up with some results, model problems are introduced, which retain only a limited number of the original features. Regarding geometry and decomposition of the 3-d problem we adopt Wu's ideas to split the actual flow into two separate, but interacting 2-d flows, namely a blade-to-blade flow and a meridional-through flow. The blade-to-blade or cascade plane is defined as a surface of revolution formed by rotating a streamline of the meridional plane about the machine's axis. Such a projection of a single blade row, and our considerations are confined to single blade rows, reveals an infinite row of equidistant, similar, airfoil-shaped bodies, called cascade. Since we do not attempt a solution of the 3-d problem, the cascade problem will be isolated from the meridional-through flow. Further we do not allow any upstream disturbances, as generated by the wakes of upstream blade rows. The current calculations will also neglect the effect of viscous wakes emanating from the trailing edges of the considered blades. There is no doubt that the flow in a turbomachine is highly unsteady and even the artificial cascade problem might experience unsteadiness due to a distorted upstream flowfield. However, because our model presumes steady flow, our ability to predict stalled flows will be somewhat restricted. Our limitation to incompressible flows is mainly related to the availability of efficient inviscid cascade codes. This assumption dispenses us from taking shocks, shock reflections, and shock interactions into account. Finally the boundary layer approach imposes the restriction that viscous effects remain confined to a thin layer. Obviously, this assumption is violated in case of extensively separated flows. In view of all these drawbacks what advantages are being offered by inviscid-viscous interaction methods and why is the interaction method superior to classical boundary layer methods and purely inviscid flow solvers? The following levels of information can be associated with these procedures: Inviscid flow solvers yield a pressure distribution and the overall lift force, which can be expected to be accurate only in case of attached and high Reynolds number flows. Boundary layer methods give additional information on skin friction distribution and overall drag force, but they fail if the flow separates. Interaction methods provide pressure and skin friction distributions, lift and drag forces for attached and mildly separated flows.

The following sections will shed some light on the individual parts of this approach. The inviscid flow equations are being solved by a standard panel method, which, mathematically speaking, provides a solution of Laplace's equation subject to Neumann type boundary conditions. Singularity methods, such as the panel

method, attempt a solution by an appropriate superposition of elementary solutions, named singularities, so that the boundary condition is satisfied. In two-dimensional flows only two types of singularities are required, namely sources (and sinks) to model displacement flows, and vortices to model lift. There remains the choice where and how to distribute these singularities. Smith and Hess [13] proposed to place them on the boundary surfaces which led to the first and still very successful panel codes. The first order approximation, which we are going to use, employs a representation of the airfoil by straight-line-elements, along which singularity strengths are assumed constant. The airfoil code of Smith and Hess was extended to cascades by Giesing [9], whose approach is virtually the same as the current one, except that Giesing's method is derived and coded in complex variables, while the current one is done in real variables. Inviscid methods intended to interact with viscous flow solvers require some modifications. The commonly used flow tangency condition has to be replaced by the prescription of a wall transpiration velocity to make allowance for the displacement effect due to the existence of boundary layers.

The second building block of the scheme is the viscous flow solution, being achieved by a finite difference method. Finite difference methods are numerical tools to solve partial differential equations by discretizing the unknown functions at a limited number of gridpoints and subsequent rewriting of the differential equations in form of algebraic equations, each of which applying to an elementary subdomain. The algorithm depends on the propagation of pertubations, such that elliptic equations require expansive field solutions, while parabolic equations permit marching procedures. Hence engineers try to avoid the elliptic Navier-Stokes equations and to focus on the parabolic boundary layer equations. An order of magnitude estimation, making use of the relation that the boundary layer thickness is much smaller than the streamwise length coordinate, justifies the reduction of the elliptic Navier-Stokes equations to the parabolic boundary layer equations. However, no gain without penalties: Only flow fields which obey the boundary layer approximation ought to be treated, computations will break down at the point of zero skin friction due to the Goldstein singularity, and the downstream marching procedure will face numerical instabilities in regions of reversed flow. The first limitation is inherent to the approach. However, the Goldstein singularity is related to the boundary conditions. Catherall and Mangler [3] discovered that the boundary layer equations can be integrated through the point of separation, if displacement thickness or wall shear stress is prescribed instead of the external velocity. The third problem is tricky because of both up- and downstream propagating pertubations, which revert the problem locally to an elliptic one. The most common remedy, the so-called FLARE approximation [19], drops the streamwise convective term in regions of backflow, thus getting rid of the numerical instabilities, but violating the physics whenever backflow velocities exceed small values. After having discussed the basic advantages and disadvantages of boundary layer methods, we continue with information on the currently employed method. Our viscous flow solution features Keller's box method [14], which is implicit and second order accurate. In regions where separation is unlikely to occur the boundary layer equations are recast in terms of Falkner-Skan variables and solved subject to prescribed external velocities. This direct method, which is applied in the immediate neighbourhood of the leading edge only, exhibits the classical hierarchical structure between viscous and inviscid flow regions, indicating that the outer flow imposes the pressure on the viscous layer. Soon after the leading edge or at the pressure peak, at the latest, the scheme switches from the direct to the interactive mode, which ensures the mutual interaction of inner and outer flow. While direct methods specify the pressure and inverse methods the displacement thickness, neither of these is prescribed in an interactive boundary condition. Both external velocity and displacement thickness are treated as unknowns and the boundary condition specifies a relation between the unknown streamfunction at the boundary layer edge, external velocity and displacement thickness. The concept of nearly constant boundary layer thickness, as provided by Falkner-Skan variables, has to be abandoned. The boundary layer equations are now written in terms of physical transformed coordinates and the Mechul function method by Cebeci accounts for the status of the external velocity as an unknown variable. Besides the crucial boundary condition at the outer edge of the viscous layer both methods employ the no-slip condition at the wall and the direct method requires initial conditions, which are generated by similarity solutions.

In order to compute turbulent flows knowledge about Reynolds stresses, specifically turbulent shear stresses, is necessary. Unfortunately our understanding of turbulence is still quite inadequate. Therefore, we must use simple models based on hypotheses. The currently used model, the eddy viscosity concept by Cebeci and Smith [4], relates the turbulent shear stresses to mean flow properties on an empirical basis. This algebraic zero-equation closure allows to retain the same form of the differential equations and to apply the

same numerical procedures to both laminar and turbulent flows. In order to know where to start turbulent flow computations prediction of transition is necessary. Since again no exact methods are available, the best choice is to take experimental results. The attempt to predict transition is still in its infancy, resulting in rather limited applicability. Michel's method, which is used here, is based upon an empirical data correlation, narrowing considerably the range of applicability, while linear stability theories with empirical assumptions, like the e^9-method offer some universality. Probably, transition and turbulence modelling represent the weakest members in the computational scheme.

The interaction term describes the way how the inner viscous and outer inviscid regions communicate with each other. The transmitter of any information is obviously the edge boundary condition, which in case of a weak interaction works out as follows: The result of the inviscid flow computation, which is the pressure distribution, is imposed as boundary condition on the viscous flow computation. In return the result of the viscous flow solution, which is the displacement thickness, determines the effective shape of the body which is input to the inviscid flow solver. Basically, there are two possibilities to account for the displacement effect of a boundary layer on the outer inviscid flow: Either the blades are thickened by adding the displacement thickness to the blade coordinates or the flow tangency condition on the blade is substituted by a condition which prescribes a blowing velocity. Both ways can be incorporated either in a weak or strong interaction. A weak interaction will be sufficient if the viscous effect on the pressure is small, permitting the above described, hierarchical manner of solving the complete flow problem. However, there are regions, like the trailing edge and separated flow, where viscous displacement might cause more severe changes in the local pressure field so that alternating treatment of external velocity and displacement thickness as in- and output appears to be too rigid a mechanism for the interaction of viscous and inviscid flow regimes. These sensitive areas call for equivalent and simultaneous treatment of displacement thickness and external velocity. Schemes, which meet these standards and hence do not possess a definite hierarchy, are named strong interaction models. Only they are capable of calculating boundary layers with flow separation. The approach taken here follows closely the ideas of Veldman [22], who initially introduced the concept of strong interaction.

The global organization of the scheme (see figure 1 on page 4) shows an iterative process in which alternately inviscid and viscous flow equations are being solved. Results are considered as converged if the external velocity distributions of viscous and inviscid flow solutions do coincide and if the results of the viscous flow solutions do remain steady over consecutive iteration cycles. Relaxation is a numerical tool either to ensure or to accelerate convergence. Viscous flow results are updated by relaxation just before they are transferred to the inviscid flow solver to serve there as boundary condition. The actually used relaxation formula was proposed by Kwon and Pletcher [15] and allows overrelaxation.

The present report expands upon the work of Cebeci et al. [8], who developed a viscous-inviscid interaction method for incompressible cascade flows. The objective of the present work is to provide a complete description of the theory and to conduct a few sample calculations in order to begin the evaluation procedure. In chapter 2 a description of the panel method is given which is used to compute incompressible inviscid flows through arbitrarily staggered cascades of arbitrarily shaped blade sections. The solution of the boundary layer equations subject to an imposed pressure as well as to an interactive edge condition is discussed in chapter 3, which, additionally, reviews the used interaction and turbulence models. Flow results in form of pressure, skin friction, displacement thickness, and velocity profiles are presented and analysed in chapter 4 for the NACA-65-series compressor blade family. The cascade configuration, namely a stagger angle of 45 degrees and a blade solidity of 0.78, was selected in consideration of available experimental data. Calculations were performed for Reynolds numbers of 245 thousand and 6 million and for air inlet angles ranging from 40 to 62 degrees. The report closes with a brief summary and recommendations for future work. The reader is alerted to the fact that the present report is of an interim nature covering the period September 1985 through August 1986.

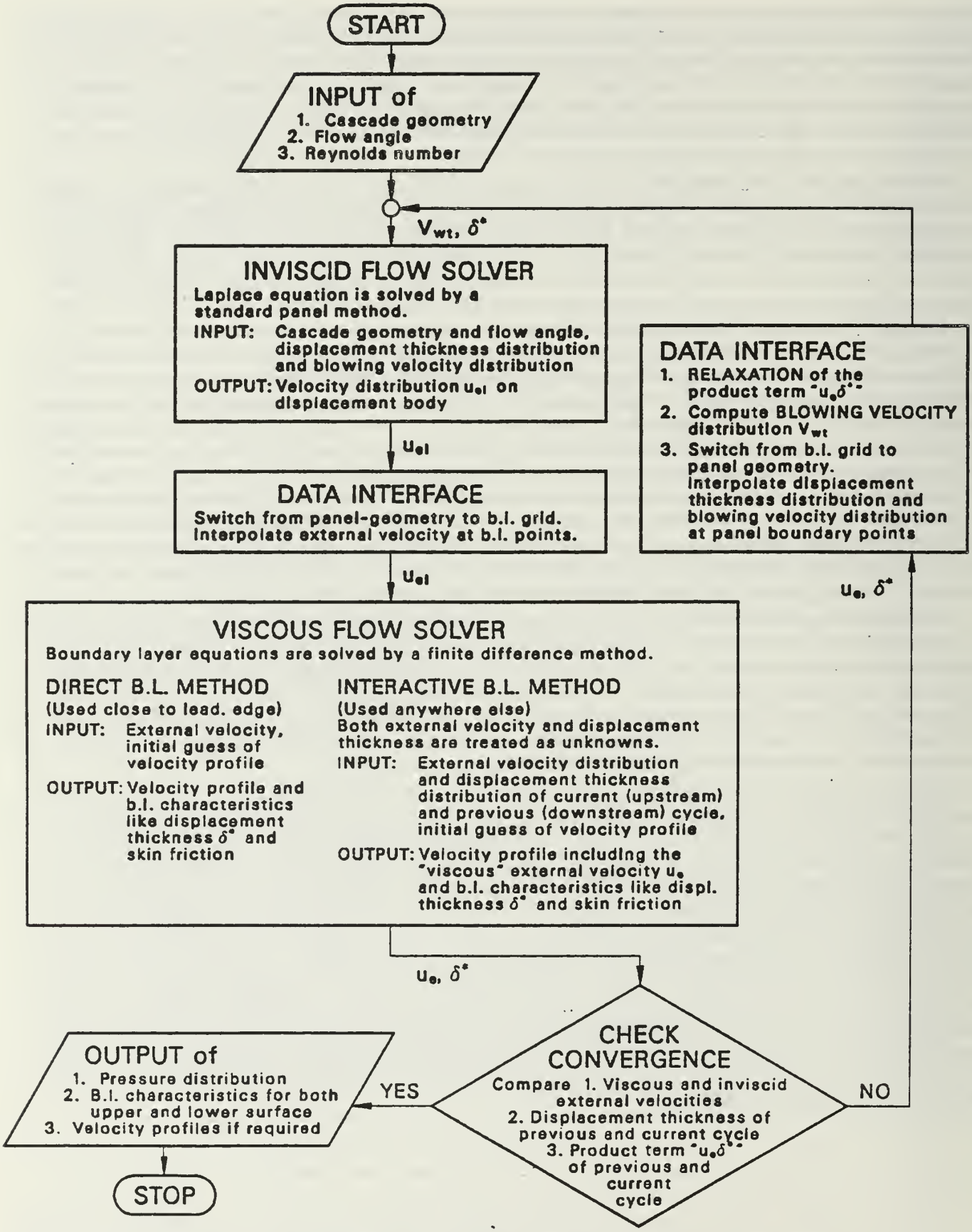

Fig. 1. Global organization of viscous-inviscid interaction method

2. INVISCID FLOW METHOD

Since the outer flow is assumed to be incompressible, a solution of Laplace's equation will provide inviscid flow results. Laplace's equation will be subject to a Neumann type boundary condition, which prescribes a blowing velocity on the surface of the blades, resulting from the viscous displacement effect. In addition Kutta's condition, postulating zero load at the trailing edge, is imposed to establish a unique solution. The numerical implementation requires a couple of approximations which are associated with the term panel method. The following sections will cover a description of singularity methods in potential flows. the definition of the inviscid cascade problem, the concepts of influence coefficients and basic flows. and the derivation of farfield cascade relations enabling the statement of Kutta's condition for given inlet angle of attack and the calculation of inlet and exit flow conditions.

2.1 Singularity methods in potential flows

Irrotational flow fields ($curl\,\vec{V} = \vec{0}$) permit that the velocity vector may be expressed as the gradient of a scalar function, called the velocity potential Φ,

$$\vec{V} = grad\,\Phi.$$

This definition together with the principle of conservation of mass for incompressible flows ($div\,\vec{V} = 0$) yields Laplace's equation,

$$div\,(grad\,\Phi) = 0 \qquad \text{or} \qquad \Delta\Phi = 0$$

which governs the steady flow field of incompressible inviscid fluids. The commonly used flow tangency condition is replaced here by a boundary condition that specifies a wall transpiration velocity

$$\frac{\partial\Phi}{\partial n} = V_{wt}(s) \qquad \text{on the surface of blades}$$

Laplace's equation is a linear homogeneous second order partial differential equation. which is classified as elliptic. demanding a field solution. Two concepts have proven successful in the exact solution of Laplace's equation. the method of separation of variables and singularity methods. The latter ones achieve a solution by an appropriate superposition of elementary solutions. called singularities. This technique. underlying all panel codes. is based on Green's theorem and the principle of superposition. which applies to any linear partial differential equation

$$\text{If } \Delta\Phi_1 = 0.\ \Delta\Phi_2 = 0.\ldots.\ \Delta\Phi_n = 0.\ldots.\Delta\Phi_N = 0$$
$$\text{then } \Delta\Phi = 0 \text{ with } \Phi = C_1\Phi_1 + C_2\Phi_2 + \ldots + C_n\Phi_n + \ldots + C_N\Phi_N$$

where $C_1, C_2, \ldots, C_n, \ldots,$ and C_N denote arbitrary constants. Green's theorem. which is specific to Laplace's equation. states that the flow past arbitrarily shaped bodies may be represented by surface singularity distributions. This theorem simplifies the solution procedure considerably. because the flow at a field point can be computed by summing up the effects of all singularities instead of all field points. For 2-d flows the singularities to be used are sources and vortices. because the effect of displacement and thickness. respectively. can be handled by distributions of sources and sinks. while the effect of lift is modelled by a distribution of vortices. The name singularity is attached to sources and vortices. because they do satisfy Laplace's equation everywhere except at a singular point.

Since the overall flow will be built up by simple flows. we review first the velocity potentials of basic flows which constitute the elements of our flow synthesis. The velocity potential of uniform parallel flow that is inclined with respect to the positive x-axis by an angle α is given by

$$\varphi(x, y) = U_\infty(x\cos\alpha + y\sin\alpha)$$

where U_∞ denotes the magnitude of the constant velocity vector. Radial streamlines and concentric circular equipotentials characterize the flow field of a single source

$$\varphi(x, y) = \frac{\sigma}{2\pi}\ln\sqrt{x^2 + y^2}$$

where σ denotes the source strength and the source is located at (0,0). Interchanging streamlines and equipotentials of a single source produces the flow field of a single vortex

$$\varphi(x,y) = -\frac{\gamma}{2\pi}\arctan\frac{y}{x}$$

where a positive γ denotes the strength of a clockwise rotating vortex, located at (0,0). Our principal interest is in cascade flows so that our further considerations will deal with infinite rows of singularities. The velocity potential of an infinite row of equal and equidistant sources at the points $(0,0)$, $(0,\pm\tau)$, $(0,\pm 2\tau)$, $(0,\pm 3\tau)$,... can be expressed in terms of hyperbolic and trigonometric functions

$$\varphi(x,y) = \frac{\sigma}{2\pi}\sum_{k=+\infty}^{k=+\infty}\ln\sqrt{x^2+(y-k\tau)^2} = \frac{\sigma}{2\pi}\ln\left[\frac{1}{2}\left(\cosh\frac{2\pi x}{\tau}-\cos\frac{2\pi y}{\tau}\right)\right]$$

A similar process leads to the velocity potential of an infinite row of equal and equidistant vortices at the points $(0,0)$, $(0,\pm\tau)$, $(0,\pm 2\tau)$, $(0,\pm 3\tau)$,...

$$\varphi(x,y) = -\frac{\gamma}{2\pi}\sum_{k=+\infty}^{k=+\infty}\arctan\frac{y-k\tau}{x} = -\frac{\gamma}{2\pi}\arctan\left(\frac{\tan\frac{\pi y}{\tau}}{\tanh\frac{\pi x}{\tau}}\right)$$

2.2 Cascade flows

Recalling that a cascade is defined as an infinite row of equidistant similar airfoil shaped bodies, we can conclude that the flow field past a cascade, which is inclined to a uniform steady onset flow, consists of identical subflowfields, each of which is enclosed by two streamlines being displaced at the cascade's spacing. Identical subflowfields obviously can be caused only by identical singularity distributions on each body, so that the above defined infinite series will replace the expressions for single source and vortex as used in the airfoil formulae. On the basis of Laplace's equation's linearity we decompose the total velocity potential Φ into that of uniform onset flow and the so-called disturbance potential φ, which accounts for the disturbance by the cascade of an originally uniform flow field

$$\Phi(x,y) = U_\infty(x\cos\alpha + y\sin\alpha) + \varphi(x,y)$$

where U_∞ and α are magnitude and direction (with respect to positive x-axis) of the vector mean velocity. (Note: The vector mean velocity is defined as the vector average of inlet and exit velocity vector). The disturbance velocity potential of a cascade , whose blades are arranged along the y-axis, can be written as

$$\varphi(x,y) = \int_{S_0}\left\{\frac{\sigma(s)}{4\pi}\ln\left[\frac{1}{2}\left(\cosh\frac{2\pi}{\tau}(x-x_0(s))-\cos\frac{2\pi}{\tau}(y-y_0(s))\right)\right] - \frac{\gamma}{2\pi}\arctan\left(\frac{\tan\frac{\pi}{\tau}(y-y_0(s))}{\tanh\frac{\pi}{\tau}(x-x_0(s))}\right)\right\}ds$$

where the integration is carried out along the surface of the center blade, (x_0, y_0) denotes the coordinates of the center blade, and τ is the vertical spacing between adjacent blades. Since this integration cannot be performed analytically for arbitrarily shaped blades, the continuos singularity distributions are discretized in the following fashion:

1. Blades will be represented by straight line panels.
2. The boundary condition will be satisfied at the midpoints of panels.
3. Source strengths are assumed constant along each panel, but vary from panel to panel. Vortex strengths are constant over the blade.

This unequal status of source and vortex strengths is due to the requirement that the number of unknowns must balance the number of equations. If the blade is approximated by N panels, N boundary conditions applied at the midpoints of the N panels, plus Kutta's condition at the trailing edge produce equations for $N+1$ unknowns. Hence the N unknown source strenghts are determined such that the boundary

conditions are satisfied, while there is only one equation left to adjust one vortex strength. Introducing these approximations to the disturbance potential we get

$$\varphi(x,y) = \sum_{j=1}^{N} \frac{\sigma_j}{4\pi} \int_{-l_j/2}^{+l_j/2} \ln\left[\frac{1}{2}\left(\cosh\frac{2\pi}{\tau}(x-x_j-s\cos\theta_j) - \cos\frac{2\pi}{\tau}(y-y_j-s\sin\theta_j)\right)\right] ds$$

$$- \frac{\gamma}{2\pi} \sum_{j=1}^{N} \int_{-l_j/2}^{+l_j/2} \arctan\left(\frac{\tan\frac{\pi}{\tau}(y-y_j-s\sin\theta_j)}{\tanh\frac{\pi}{\tau}(x-x_j-s\cos\theta_j)}\right) ds$$

where σ_j denotes the source strength of the j-th panel
γ the vortex strength, which is constant for all panels
(x_j, y_j) are the coordinates of the midpoint of the j-th panel
l_j and θ_j denote length of the j-th panel and the angle (positive counterclockwise) between surface direction of the j-th panel (positive clockwise) and positive x-axis.

2.3 Concept of influence coefficients

Eventually we are concerned with velocities rather than the potential which is merely a vehicle to give information on the velocity field. Remembering that the velocity vector is the gradient of the potential, we can apply this operator in any convenient reference coordinate system including local coordinate systems attached to panels. Now there are two velocity components we need to know: Firstly, normal velocities at panel-midpoints are required to satisfy the boundary conditions and secondly, tangential velocites are necessary to compute the pressure distribution on the blades. Both velocities will be computed by separately taking into account the influence of each panel resulting in $2N$ contributions, one half induced by source distributions, the other half induced by vortex distributions. This procedure, called concept of influence coefficients, constitutes the numerical core of the panel method. Influence coefficients are hence defined as velocities induced by a unit singularity distribution of one panel. Let n_i and t_i be outer normal and clockwise tangential directions at the midpoint (x_i, y_i) of the i-th panel, then influence coefficients due to source distributions take the form:

A_{ij} represents the outer normal velocity at (x_i, y_i) induced by a unit source distribution on the j-th panel

$$A_{ij} = \frac{1}{4\pi} \int_{-l_j/2}^{+l_j/2} \frac{\partial}{\partial n_i}\left\{\ln\left[\frac{1}{2}\left(\cosh\frac{2\pi}{\tau}(x_i-x_j-s\cos\theta_j) - \cos\frac{2\pi}{\tau}(y_i-y_j-s\sin\theta_j)\right)\right]\right\} ds$$

$$= -\sin(\theta_i-\theta_j)\,V_{x_{ij}} + \cos(\theta_i-\theta_j)\,V_{y_{ij}} \qquad \text{for } i \neq j$$

$$A_{ij} = \frac{1}{2} \qquad \text{for } i = j$$

B_{ij} represents the clockwise tangential velocity at (x_i, y_i) due to a unit source distribution on the j-th panel

$$B_{ij} = \frac{1}{4\pi} \int_{-l_j/2}^{+l_j/2} \frac{\partial}{\partial t_i}\left\{\ln\left[\frac{1}{2}\left(\cosh\frac{2\pi}{\tau}(x_i-x_j-s\cos\theta_j) - \cos\frac{2\pi}{\tau}(y_i-y_j-s\sin\theta_j)\right)\right]\right\} ds$$

$$= \cos(\theta_i-\theta_j)\,V_{x_{ij}} - \sin(\theta_i-\theta_j)\,V_{y_{ij}} \qquad \text{for } i \neq j$$

$$B_{ij} = 0 \qquad \text{for } i = j$$

with

$$V_{x_{ij}} = \frac{1}{4\pi} \ln \frac{\cosh^2\frac{\pi(x_i-X_j)}{\tau} - \cos^2\frac{\pi(y_i-Y_j)}{\tau}}{\cosh^2\frac{\pi(x_i-X_{j+1})}{\tau} - \cos^2\frac{\pi(y_i-Y_{j+1})}{\tau}}$$

$$V_{y_{ij}} = \frac{1}{2\pi}\left\{\arctan\Lambda_1 + \arctan\Lambda_2 - \arctan\Lambda_3\right\}$$

where the arguments Λ_1, Λ_2, Λ_3 are given by

$$\Lambda_1 = \frac{[-(x_i-X_j)\sin\theta_j + (y_i-Y_j)\cos\theta_j]l_j}{(x_i-X_j)^2 + (y_i-Y_j)^2 - l_j[(x_i-X_j)\cos\theta_j + (y_i-Y_j)\sin\theta_j]}$$

$$\Lambda_2 = \frac{\frac{\pi(x_i-X_{j+1})}{\pi}\cosh\frac{\pi(x_i-X_{j+1})}{\pi}\sin\frac{\pi(y_i-Y_{j+1})}{\pi} - \frac{\pi(y_i-Y_{j+1})}{\pi}\sinh\frac{\pi(x_i-X_{j+1})}{\pi}\cos\frac{\pi(y_i-Y_{j+1})}{\pi}}{\frac{\pi(x_i-X_{j+1})}{\pi}\sinh\frac{\pi(x_i-X_{j+1})}{\pi}\cos\frac{\pi(y_i-Y_{j+1})}{\pi} + \frac{\pi(y_i-Y_{j+1})}{\pi}\cosh\frac{\pi(x_i-X_{j+1})}{\pi}\sin\frac{\pi(y_i-Y_{j+1})}{\pi}}$$

$$\Lambda_3 = \frac{\frac{\pi(x_i-X_j)}{\pi}\cosh\frac{\pi(x_i-X_j)}{\pi}\sin\frac{\pi(y_i-Y_j)}{\pi} - \frac{\pi(y_i-Y_j)}{\pi}\sinh\frac{\pi(x_i-X_j)}{\pi}\cos\frac{\pi(y_i-Y_j)}{\pi}}{\frac{\pi(x_i-X_j)}{\pi}\sinh\frac{\pi(x_i-X_j)}{\pi}\cos\frac{\pi(y_i-Y_j)}{\pi} + \frac{\pi(y_i-Y_j)}{\pi}\cosh\frac{\pi(x_i-X_j)}{\pi}\sin\frac{\pi(y_i-Y_j)}{\pi}}$$

$V_{x_{ij}}$ and $V_{y_{ij}}$ denote x- and y-components (in a local coordinate system, whose x- and y-axes point in the clockwise tangential and outer normal directions of the j-th panel) of the velocity at (x_i, y_i), induced by a unit source distribution of the j-th panel. Coordinates of boundary points (X_j, Y_j) and midpoints (x_j, y_j) are related by

$$x_j = \frac{1}{2}(X_j + X_{j+1}) = X_j + \frac{l_j}{2}\cos\theta_j$$

$$y_j = \frac{1}{2}(Y_j + Y_{j+1}) = Y_j + \frac{l_j}{2}\sin\theta_j$$

Potential flow solutions frequently encounter troubles because of the multivalued arctangent. The following two provisions make sure that the arctangent, and subsequently the induced velocity, do not jump in value, where it is not supposed to do so: All arctangents must be evaluated in the range $-\pi$ to $+\pi$ and $V_{y_{ij}}$ is calculated by adding up the effect of a single airfoil, given by the first term, and the effect of a cascade without the center blade, represented by the second and third term. A minor difficulty, the computation of velocities at the midpoint of the inducing panel, can be overcome by Cauchy's principal value technique, which permits integration of certain singular integrands.

The influence coefficients due to a vortex distribution can be related to those due to a source distribution. Based on the fact that velocity fields of vortex and source are different by a clockwise rotation of 90 degrees only, the normal velocity due to a vortex equals the negative tangential velocity due to a source, and the tangential velocity due to a vortex equals the normal velocity due to a source

$$A_{ij}^{VORTEX} = -B_{ij}^{SOURCE}$$

$$B_{ij}^{VORTEX} = A_{ij}^{SOURCE}$$

(Unless indicated otherwise influence coefficients will be those due to a source distribution.)

2.4 Concept of basic flows

Equipped with the concept of influence coefficients we can now deal with the satisfaction of the boundary condition, which is to determine source and vortex strengths such that velocities of given magnitude and direction be induced at panel midpoints:

$$\frac{\partial\Phi(x_i, y_i)}{\partial n_i} = (V_{wt})_i \qquad \text{for } i = 1.....N$$

$$\sum_{j=1}^{N} A_{ij}\sigma_j^{(0)} - \gamma\sum_{j=1}^{N} B_{ij} = (V_{wt})_i + U_\infty(\sin\theta_i\sin\alpha - \cos\theta_i\cos\alpha) \qquad \text{for } i = 1.....N$$

To match the $N+1$ unknowns (N source and 1 vortex strength) by an equal number of equations the system is complemented by the empirical Kutta's condition. The resulting system could be solved in a straightforward fashion by a linear equation algorithm: however, traditionally the flow is split into three basic flows, thus providing a very efficient solution for different angles of attack in case of no wall transpiration. Basic flows naturally divide into displacement and lift generating flows as follows:

1. Zero angle of attack flow ($\alpha = 0$ deg, $\gamma = 0$, wall transpiration):

$$\sum_{j=1}^{N} A_{ij}\sigma_j^{(0)} = \frac{(V_{wt})_i}{\cos\alpha} + U_\infty \sin\theta_i \qquad \text{for } i = 1,\ldots,N$$

2. Ninety degrees angle of attack flow ($\alpha = 90$ deg, $\gamma = 0$, no wall transpiration):

$$\sum_{j=1}^{N} A_{ij}\sigma_j^{(90)} = -U_\infty \cos\theta_i \qquad \text{for } i = 1,\ldots,N$$

3. Purely circulatory flow ($U_\infty = 0$, $\gamma = 1$, no wall transpiration):

$$\sum_{j=1}^{N} A_{ij}\sigma_j^{(\gamma)} = \sum_{j=1}^{N} B_{ij} \qquad \text{for } i = 1,\ldots,N$$

Each of the above equations stands for a system of N equations with unknown source strengths only. Since all systems show up with the same coefficient matrix, the three sets of source strengths can be obtained by one execution of a linear equation solver with three different right hand sides. Although the concept of basic flows is primarily a numerical tool the following physical interpretation can be given: The first basic flow represents a pure displacement flow, whereby blades are inclined at zero angle of attack (angle with respect to global x-axis, not blade chordline). The boundary condition of the first basic flow consists in a prescription of a wall transpiration velocity. The second basic flow is also a pure displacement flow, but at an angle of attack of ninety degrees and subject to a no-penetration condition. The third basic flow represents a purely circulatory flow. Since a constant vortex distribution alone would not obey the flow tangency condition, normal velocities induced by this constant vortex distribution are balanced by an extra source distribution. In summary: Each of the basic flows satisfies some kind of boundary condition and each of them violates Kutta's condition. An appropriate linear combination of all three basic flows will yield flow at the required angle of attack subject to Kutta's condition:

Total flow = "Zero angle of attack flow" * $\cos\alpha$
+ "Ninety degrees angle of attack flows" * $\sin\alpha$
+ "Purely circulatory flow" * γ

The vortex strength γ is still unknown in the above equation, but provided it is known, total normal and tangential velocities at the midpoint of the i-th panel take the following form

$$V_n(x_i, y_i) = \frac{\partial\Phi(x_i, y_i)}{\partial n_i} = U_\infty \sin(\alpha - \theta_i) + \sum_{j=1}^{N} A_{ij}\sigma_j - \gamma \sum_{j=1}^{N} B_{ij}$$

$$V_t(x_i, y_i) = \frac{\partial\Phi(x_i, y_i)}{\partial t_i} = U_\infty \cos(\alpha - \theta_i) + \sum_{j=1}^{N} B_{ij}\sigma_j + \gamma \sum_{j=1}^{N} A_{ij}$$

with $\sigma_j = \sigma_j^{(0)} \cos\alpha + \sigma_j^{(90)} \sin\alpha + \sigma_j^{(\gamma)}\gamma$. The deviation of the outer normal velocities V_n from the prescribed wall transpiration velocities V_{wt} is a measure of the accuracy of the linear equation solver.

2.5 Farfield cascade relations

For farfield considerations the flowfield past a cascade can be simulated by an infinite row of discrete vortices. Such an approach can be justified because the displacement-disturbances decay with increasing up- and downstream distance and because there remains a finite effect due to circulation in the farfield. Using the formerly defined velocity potential of an infinite row of equal and equidistant vortices, this simplified model produces information about the horizontal and vertical disturbance velocities in the farfield of a cascade

$$u_1 = u_2 = \lim_{x \to \mp\infty} \left\{ \frac{\partial}{\partial x} \left[-\frac{\Gamma}{2\pi} \arctan\left(\frac{\tan\frac{\pi y}{t}}{\tanh\frac{\pi x}{t}} \right) \right] \right\} = 0$$

$$v_{\frac{1}{2}} = \lim_{x \to \mp\infty} \left\{ \frac{\partial}{\partial y} \left[-\frac{\Gamma}{2\pi} \arctan\left(\frac{\tan\frac{\pi y}{t}}{\tanh\frac{\pi x}{t}} \right) \right] \right\} = \pm\frac{\Gamma}{2\pi}$$

where the small letters u and v denote the components of disturbance velocities, and the subscripts 1 and 2 indicate streamwise positions at up- and downstream infinity. Magnitudes and angles of total inlet and exit velocities can be obtained by superposition of the above disturbance flowfield and a uniform paralell flowfield, which is inclined by an angle of α

$$\text{Abs(Inlet velocity):} \quad \sqrt{U_1^2 + V_1^2} = \sqrt{(U_\infty \cos\alpha + u_1)^2 + (U_\infty \sin\alpha + v_1)^2}$$
$$= \sqrt{U_\infty^2 + \left(\frac{\Gamma}{2r}\right)^2 + \frac{U_\infty \sin\alpha\, \Gamma}{r}}$$

$$\text{Air inlet angle:} \quad \tan\alpha_1 = \frac{V_1}{U_1} = \frac{U_\infty \sin\alpha + \Gamma/(2r)}{U_\infty \cos\alpha}$$

$$\text{Abs(Outlet velocity):} \quad \sqrt{U_2^2 + V_2^2} = \sqrt{U_\infty^2 + \left(\frac{\Gamma}{2r}\right)^2 - \frac{U_\infty \sin\alpha\, \Gamma}{r}}$$

$$\text{Air outlet angle:} \quad \tan\alpha_2 = \frac{V_2}{U_2} = \frac{U_\infty \sin\alpha - \Gamma/(2r)}{U_\infty \cos\alpha}$$

where the capital letters U and V designate the components of total velocities and U_∞ is the magnitude of the vector mean velocity. (For an illustration of angles and velocity components see figure 2 on page 12).

The calculation of forces requires either a pressure integration along the blade or the application of the momentum equation in integral form to an appropriate control surface. The latter method is to be preferred here because it involves fewer numerical steps and is said to be more accurate for small numbers of panels. Assuming steady 2-d flows of incompressible fluids the momentum equation can be written according to

$$\vec{F} = (F_x, F_y)^T = -\rho \oint_C \vec{V}(\vec{V}\vec{n})\, ds - \oint_C p\vec{n}\, ds$$

where C denotes the control surface consisting of two vertical planes in the up- and downstream farfield and two similar streamlines, which are arranged such that they enclose a single blade. Making use of Bernoulli's equation magnitude and direction of the resultant gross force per unit span become

$$F = \sqrt{F_x^2 + F_y^2} = \rho U_\infty \Gamma \qquad \text{with} \quad U_\infty = \sqrt{U_1^2 + ((V_1 + V_2)/2)^2}$$

$$\epsilon = \arctan(F_y/F_x) = \alpha + 90 \text{ degrees}$$

The gross force turns out to act at a right angle relative to vector mean velocity, while no force is exerted in the direction of vector mean velocity. Lift is defined as the force perpendicular to vector mean velocity. Normalizing this force by a reference area and the dynamic pressure, based either on vector mean or inlet velocity, gives the dimensionless lift coefficient

$$C_L = \frac{F}{c_{ref}(\rho U_{ref}^2/2)} = \frac{2U_\infty \Gamma}{c_{ref} U_{ref}^2}$$

2.6 Kutta's condition

Kutta's condition assures that flows on the upper and lower surfaces merge smoothly at the trailing edge by postulating equal pressures and subsequent equal velocities there. Since the panel method does not permit the evaluation of velocities at boundary points, Kutta's condition is satisfied in an approximate fashion at the control points of the first and last panel

$$V_{t_1} = -V_{t_N}$$

This condition determines the vortex strength γ, whose knowledge is necessary to synthesize the combined flow. Hence the scheme makes use of Kutta's condition after completing the basic flow solution and before

starting the combined flow computation. Cascade flows offer several input possibilities, two of which are being considered here. For a given average onset flow angle Kutta's condition is a linear equation in the unknown vortex strength γ

$$U_\infty \left[\cos(\alpha - \theta_1) + \cos(\alpha - \theta_N)\right] + \sum_{j=1}^{N} \left[(B_{1j} + B_{Nj})(\cos\alpha\, \sigma_j^{(0)} + \sin\alpha\, \sigma_j^{(90)})\right]$$
$$= -\gamma \left[\sum_{j=1}^{N} (B_{1j} + B_{Nj})\sigma_j^{(\gamma)} + \sum_{j=1}^{N} (A_{1j} + A_{Nj})\right]$$

For given inlet air angle two unknowns, average onset flow angle α and vortex strength γ, remain to be determined, resulting in the need for another relation. Kutta's condition and the equation for the inlet air angle constitute a linear system in the two unknowns $\gamma/\cos\alpha$ and $\tan\alpha$, which can be solved by any suitable procedure

$$\left[U_\infty(\sin\theta_1 + \sin\theta_N) + \sum_{j=1}^{N} (B_{1j} + B_{Nj})\sigma_j^{(90)}\right]\tan\alpha + \left[\sum_{j=1}^{N} (B_{1j} + B_{Nj})\sigma_j^{(\gamma)} + \sum_{j=1}^{N} (A_{1j} + A_{Nj})\right]\frac{\gamma}{\cos\alpha}$$
$$= -U_\infty\left[\cos\theta_1 + \cos\theta_N\right] - \sum_{j=1}^{N} (B_{1j} + B_{Nj})\sigma_j^{(0)}$$

$$U_\infty \tan\alpha + \frac{\Sigma l_j}{2r}\frac{\gamma}{\cos\alpha} = U_\infty \tan\alpha_1$$

One possibility to increase accuracy, especially if there are lower limits on the panel length at the trailing edge, is extrapolation of velocities at the trailing edge. This approach avoids the problem regarding singular behaviour of velocities at panel boundary points, and allows to impose Kutta's condition exactly at the trailing edge. In case of linear extrapolation Kutta's condition can be written as

$$V_{t_1} + \frac{V_{t_1} - V_{t_2}}{l_1 + l_2} l_1 = -V_{t_N} - \frac{V_{t_N} - V_{t_{N-1}}}{l_N + l_{N-1}} l_N$$

where the indices 1 and N refer to the first and last panel, with numbering starting at the trailing edge on the lower surface and ending there on the upper surface.

If the displacement effect due to the boundary layer is accounted for (nonzero wall transpiration velocity), it is advisable to evaluate the pressure distribution on the displacement surface itself. This step has to be taken because if the wall transpiration velocity exceeds small values, the assumption of no pressure gradient accross the ficticious inviscid flow region between blade and displacement surface ceases to be valid. The displacement surface is therefore the location, where total velocities are to be computed and where Kutta's condition is to be met. While the scheme up to and including the calculation of basic flows remains unchanged, the scheme then proceeds with the computation of two more sets of influence coefficients. These so-called off-body influence coefficients represent normal and tangential velocities on the displacement surface induced by source and vortex distibutions of unit strength, residing on the original blade surface. The scheme makes use of these coefficients in determining circulation by imposing Kutta's condition off-body at the trailing edge and computing total velocities. On the assumption of a rigorous (inviscid) theory the displacement surface will not be penetrated by fluid particles. However, because the computation of the blowing velocities is based upon a flat plate model, total velocities on the displacement surface have a tangential velocity component and a nonzero normal velocity component, which is smaller by an order of magnitude. The magnitude of the total velocities multiplied by the sign of the tangential component are transferred to the viscous flow solver.

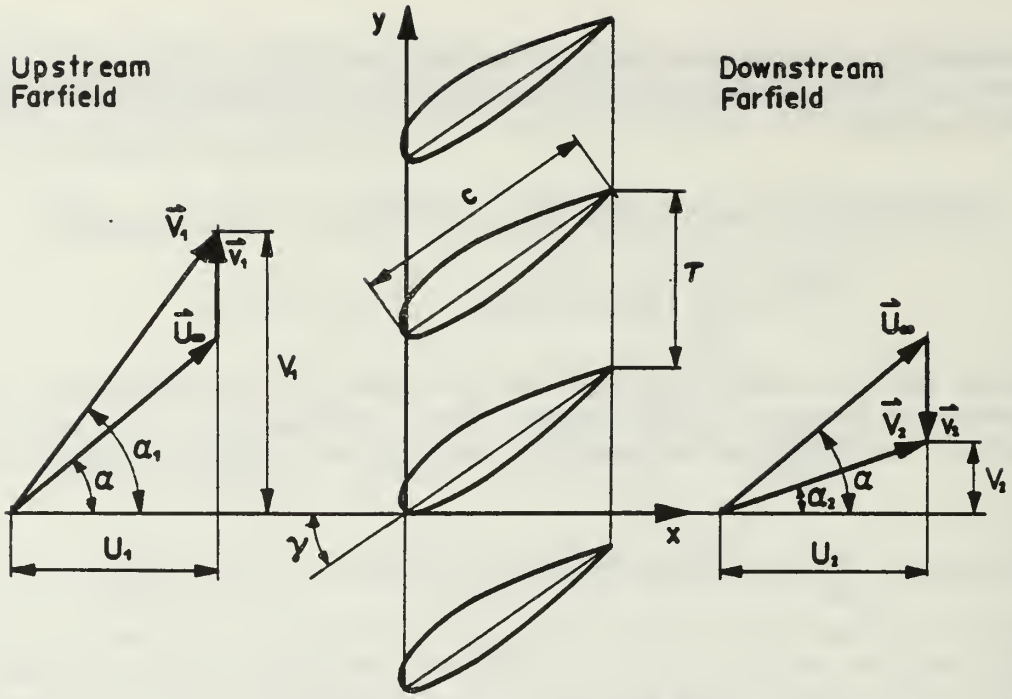

Fig. 2. Cascade geometry and its vector diagrams

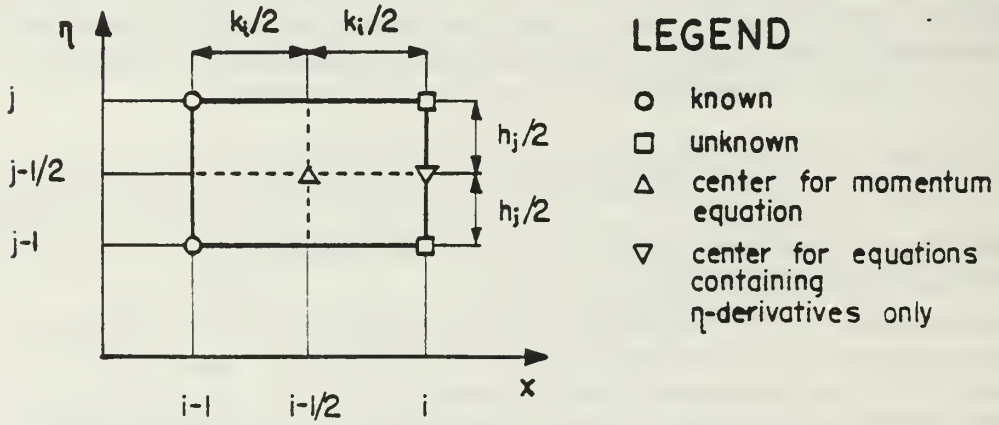

Fig. 3. Net rectangle for finite difference approximations

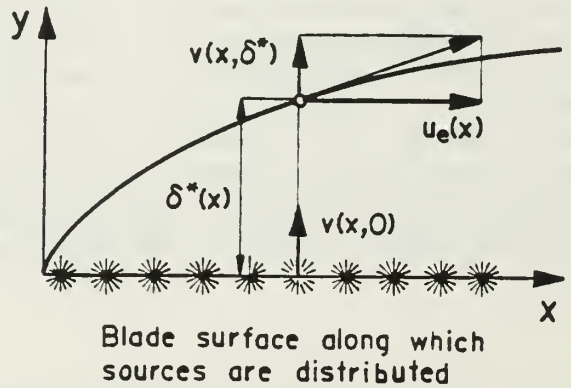

Fig. 4. Visualization of the blowing velocity concept

3. VISCOUS FLOW METHOD

In 1904 L. Prandtl gave birth to boundary layer theory, which closed the gap between the exact science of hydrodynamics and the more engineering-orientated hydraulics. Prandtl showed that the flow field past a body can be divided into two regions :

1. a thin layer close to the surface of the body and the ensuing wake, where viscous effects have to be accounted for, and
2. the remaining region, where inertia terms are dominant over viscous terms so that the latter may be neglected.

These simplifications turn the elliptic Navier-Stokes equations into the parabolic boundary layer equations, which restrain the upstream propagation of disturbances. Numerically, this change of characteristics transforms the algorithm from a field procedure to a marching method, which integrates the boundary layer equations for given initial conditions step by step proceeding in the downstream direction. The differential equations are complemented by boundary conditions, whose choice significantly influences the applicability of each scheme:

1. Direct boundary layer methods employ the so-called no-slip condition, requiring zero normal and zero tangential velocity at the surface, and a prescription of the external velocity at the edge of the boundary layer. Such procedures encounter the Goldstein singularity [10] at the point of separation, leading to a numerical breakdown.
2. Boundary layer equations can be integrated through the point of separation, if the above edge boundary condition is replaced by a prescription of either displacement thickness or wall shear stress, while the no-slip condition is kept unchanged. However, such an inverse boundary layer method coupled with an inverse inviscid flow solution suffers from very poor convergence.
3. Interactive boundary layer methods utilize an edge boundary condition which possesses the elliptic character of the outer flow. This so-called interaction law, which prescribes a linear combination of displacement thickness and external velocity, and the no-slip condition provide the required three boundary conditions for this scheme.

The numerical approach features a finite difference method, which recasts the continuity and momentum equations as a system of linear algebraic equations. Keller's box method [14] approximates derivatives by central differences and linearizes the nonlinear terms around the solution of the previous iteration. To stabilize the numerical algorithm in the presence of backflow the FLARE-approximation [19] is adopted in which the streamwise convection term is dropped in regions of backflow. The resulting set of difference equations is solved by Keller's block elimination method which takes advantage of the sparsely occupied matrix.

In the following descriptions of both direct and interactive boundary layer methods, a derivation of the interaction law, and minimum information on the turbulence model will be given. The section "Direct Boundary Layer Method" will elucidate the more basic ingredients, like discretization of the flow field and Newton's linearization, while the section on interactive boundary layer methods will emphasize its pecularities.

3.1 Direct boundary layer method

Direct methods are applicable in the absence of flow reversals, which limits their use in the current approach to the immediate neighbourhood of the leading edge. They are supposed to generate initial conditions at the stagnation point and to allow an efficient integration of the boundary layer equations around the leading edge. Generally speaking, direct methods appeal to the weak interaction problem in which viscous effects on the pressure are required to remain small. Although the paper addresses the strong interaction problem, all primary features of the finite difference method may as well be demonstrated for the direct method. To begin with we consider steady 2-d flows of incompressible fluids, described in a curvilinear coordinate system with x directing along the blade's surface and y denoting the outer normal direction. The velocity components u and v shall be determined such that they satisfy anywhere in the flowfield the equations

$$\frac{\partial u}{\partial x} + \frac{\partial v}{\partial y} = 0$$

$$u\frac{\partial u}{\partial x} + v\frac{\partial u}{\partial y} = u_e\frac{du_e}{dx} + \nu\frac{\partial}{\partial y}\left(b\frac{\partial u}{\partial y}\right)$$

and at the boundaries of the flowfield the conditions

$$y = 0: \quad u(x,0) = 0, \qquad v(x,0) = 0$$
$$y = y_e: \quad u(x,y_e) = u_e(x)$$

where b denotes $1+\nu_t/\nu$. The equations are referred to as boundary layer or thin shear layer equations, the conditions as no-slip and edge condition. In spite of the box method's requirement to reduce the governing equations to a system of first-order equations, we introduce for the present a streamfunction ($u = \partial\psi/\partial y$ and $v = -\partial\psi/\partial x$), which naturally decreases the number of dependent variables. Since streamfunctions by definition satisfy the continuity equation, only the momentum equation is left, which becomes a third order equation in ψ

$$\frac{\partial\psi}{\partial y}\frac{\partial^2\psi}{\partial x\partial y} - \frac{\partial\psi}{\partial x}\frac{\partial^2\psi}{\partial y^2} = u_e\frac{du_e}{dx} + \nu\frac{\partial}{\partial y}\left(b\frac{\partial^2\psi}{\partial y^2}\right)$$

Application of the Falkner-Skan transformation contributes to the removal of the singularity at $x = 0$ and maintains a nearly constant boundary layer thickness in terms of the new variable. In contrast to similarity concepts the dependency on two independent variables, x and η, is kept. The Falkner-Skan transformation scales the normal coordinate y and the streamfunction ψ with reference to local external velocity and local streamwise coordinate

$$\eta = \sqrt{\frac{u_e}{\nu x}}\, y$$
$$f(x,\eta) = \frac{1}{\sqrt{u_e\nu x}}\,\psi(x,y)$$

With prime denoting differentiation with respect to η the momentum equation and boundary conditions become

$$(bf'')' + \frac{m+1}{2}ff'' + m[1-(f')^2] = x\left(f'\frac{\partial f'}{\partial x} - f''\frac{\partial f}{\partial x}\right)$$
$$\eta = 0: \quad f'(x,0) = 0, \quad f(x,0) = 0$$
$$\eta = \eta_e: \quad f'(x,\eta_e) = 1$$

where $m = (x/u_e)(du_e/dx)$ is a dimensionless pressure gradient parameter.

The box method involves four steps: reduction to a first order system, discretization in terms of central differences and two-point averages, linearization, and solution of the resulting linear system. The first step is accomplished by the introduction of two additional dependent variables, U and V, which converts the third order momentum equation into a system of three first order equations

$$f' = U$$
$$U' = V$$
$$(bV)' + \frac{m+1}{2}fV + m(1-U^2) = x\left(U\frac{\partial U}{\partial x} - V\frac{\partial f}{\partial x}\right)$$

The system is complemented by the boundary conditions, which read in terms of the new variables

$$\eta = 0: \quad U(x,0) = 0, \quad f(x,0) = 0$$
$$\eta = \eta_e: \quad U(x,\eta_e) = 1$$

The second step deals with the discretization of the continuous flow problem by considering instead of the continuos functions f, U, and V a set of discrete values of these flow properties. Let the solution domain $0 \le x \le x_I$, $0 \le \eta \le \eta_J$ be covered by a rectangular mesh

$$x_1 = 0, \qquad x_i = x_{i-1} + k_i \quad \text{with} \quad 2 \le i \le I$$
$$\eta_1 = 0, \qquad \eta_j = \eta_{j-1} + h_j \quad \text{with} \quad 2 \le j \le J \quad \text{and} \quad \eta_J = \eta_e$$

Any flow property, whether it is a function or its derivative, will be expressed in terms of nodal values and coordinates of the network. Triplets of flow properties, consisting of streamfunction and its first and second derivative with respect to η, are assigned to each node of the network

$$\{f(x_i, \eta_j), U(x_i, \eta_j), V(x_i, \eta_j)\} = \{f_j^i, U_j^i, V_j^i\}$$

Because of the parabolic behaviour of the boundary layer equations the solution at a certain streamwise position, say x_i, depends solely on the solutions of upstream positions, say $x_{i-1}, x_{i-2}, \ldots$, while no downstream influence has to be considered. The overall solution works in a step-by-step fashion, propagating in the downstream direction. The use of first order equations and the technique of central differences allow to reduce the domain of dependence from all upstream x-stations to the immediate preceding one. Hence one step of the solution procedure writes the governing equations for a column of net rectangles (called boxes) residing in the subdomain

$$x_{i-1} \leq x \leq x_i \quad \text{and} \quad 0 \leq \eta \leq \eta_J$$

and solves subsequently for the nodal values at the downstream face of the rectangular shaped subdomain. The x-station being currently solved holds therefore the superscript "i", while the superscript "$i-1$" denotes the known flow properties of the adjacent upstream location. As indicated by the term central differences the equations are satisfied midway between the nodes:

The two ordinary equations are centered about $(x_i, \eta_{j-1/2})$, and
the partial equation is centered about $(x_{i-1/2}, \eta_{j-1/2})$.

The problem can now be rewritten in terms of finite differences (see figure 3 on page 12)

$$\frac{f_j^i - f_{j-1}^i}{h_j} = \frac{1}{2}(U_j^i + U_{j-1}^i)$$

$$\frac{U_j^i - U_{j-1}^i}{h_j} = \frac{1}{2}(V_j^i + V_{j-1}^i)$$

$$\frac{(bV)_j^{i-1/2} - (bV)_{j-1}^{i-1/2}}{h_j} + \left[\frac{m+1}{2}(fV)\right]_{j-1/2}^{i-1/2} + \left[m(1-U^2)\right]_{j-1/2}^{i-1/2}$$
$$= x_{i-1/2}\left[\left(U^{i-1/2}\,\frac{U^i - U^{i-1}}{k_i}\right)_{j-1/2} - \left(V^{i-1/2}\,\frac{f^i - f^{i-1}}{k_i}\right)_{j-1/2}\right]$$

Boundary conditions undergo the same discretization process and take the form

$$U_1^i = 0, \qquad f_1^i = 0$$
$$U_J^i = 1$$

One might question whether this represents a solvable system in which the number of unknowns matches the number of equations. The subdomain under consideration consists of $J-1$ net rectangles, the flow quantities of each being related by a momentum equation. Two auxiliary relations, which link dependent variables to their η-derivatives, refer to the downstream face of each net rectangle. Recalling the three boundary conditions we have a total of $3J$ equations, which face J triplets of unknowns, each of the triplets corresponding to a node of the downstream side of the rectangular subdomain. Unfortunately, the unknowns appear in nonlinear combinations, so that the solution involves an iterative procedure. The variables are linearized around their values of the preceding iteration (and in case of the first iteration around the solution of the adjacent upstream station)

$$f_j^{i,\kappa} = f_j^{i,\kappa-1} + \delta f_j^{i,\kappa} \quad \text{for } \kappa \geq 2. \qquad f_j^{i,1} = f_j^{i-1} + \delta f_j^{i,1} \quad \text{where} \quad \delta f_j^{i,\kappa} \ll f_j^{i,\kappa-1}$$
$$U_j^{i,\kappa} = U_j^{i,\kappa-1} + \delta U_j^{i,\kappa} \quad \text{for } \kappa \geq 2. \qquad U_j^{i,1} = U_j^{i-1} + \delta U_j^{i,1} \quad \text{where} \quad \delta U_j^{i,\kappa} \ll U_j^{i,\kappa-1}$$
$$V_j^{i,\kappa} = V_j^{i,\kappa-1} + \delta V_j^{i,\kappa} \quad \text{for } \kappa \geq 2. \qquad V_j^{i,1} = V_j^{i-1} + \delta V_j^{i,1} \quad \text{where} \quad \delta V_j^{i,\kappa} \ll V_j^{i,\kappa-1}$$

where κ denotes the iteration counter. If these Newton iterates are introduced and subsequently terms that are quadratic in $(\delta f_j^{i,\kappa}, \delta U_j^{i,\kappa}, \delta V_j^{i,\kappa})$ are dropped, a linear system in the unknowns $\delta f_j^{i,\kappa}$, $\delta U_j^{i,\kappa}$, $\delta V_j^{i,\kappa}$ is obtained

$$\delta f_j^{i,\kappa} - \delta f_{j-1}^{i,\kappa} - \frac{h_j}{2}(\delta U_j^{i,\kappa} + \delta U_{j-1}^{i,\kappa}) = f_{j-1}^{i,\kappa-1} - f_j^{i,\kappa-1} + h_j U_{j-1/2}^{i,\kappa-1}.$$

$$\delta U_j^{i,\kappa} - \delta U_{j-1}^{i,\kappa} - \frac{h_j}{2}(\delta V_j^{i,\kappa} + \delta V_{j-1}^{i,\kappa}) = U_{j-1}^{i,\kappa-1} - U_j^{i,\kappa-1} + h_j V_{j-1/2}^{i,\kappa-1}$$

$$(s_1)_j^{i,\kappa}\delta V_j^{i,\kappa} + (s_2)_j^{i,\kappa}\delta V_{j-1}^{i,\kappa} + (s_3)_j^{i,\kappa}\delta f_j^{i,\kappa} + (s_4)_j^{i,\kappa}\delta f_{j-1}^{i,\kappa} + (s_5)_j^{i,\kappa}\delta U_j^{i,\kappa} + (s_6)_j^{i,\kappa}\delta U_{j-1}^{i,\kappa} = (r_2)_j^{i,\kappa}$$

where the coefficients abbreviate the following expressions

$$(s_1)_j^{i,\kappa} = \frac{b_j^{i,\kappa-1}}{h_j} + \frac{x_{i-1/2}}{2k_i}\left(f_{j-1/2}^{i,\kappa-1} - f_{j-1/2}^{i-1}\right) + \frac{m^i+1}{4} f_j^{i,\kappa-1}$$

$$(s_2)_j^{i,\kappa} = -\frac{b_j^{i,\kappa-1}}{h_j} + \frac{x_{i-1/2}}{2k_i}\left(f_{j-1/2}^{i,\kappa-1} - f_{j-1/2}^{i-1}\right) + \frac{m^i+1}{4} f_{j-1}^{i,\kappa-1}$$

$$(s_3)_j^{i,\kappa} = \frac{x_{i-1/2}}{2k_i}\left(V_{j-1/2}^{i,\kappa-1} + V_{j-1/2}^{i-1}\right) + \frac{m^i+1}{4} V_j^{i,\kappa-1}$$

$$(s_4)_j^{i,\kappa} = \frac{x_{i-1/2}}{2k_i}\left(V_{j-1/2}^{i,\kappa-1} + V_{j-1/2}^{i-1}\right) + \frac{m^i+1}{4} V_{j-1}^{i,\kappa-1}$$

$$(s_5)_j^{i,\kappa} = -\left(\frac{x_{i-1/2}}{k_i} + m^i\right) U_j^{i,\kappa-1}$$

$$(s_6)_j^{i,\kappa} = -\left(\frac{x_{i-1/2}}{k_i} + m^i\right) U_{j-1}^{i,\kappa-1}$$

$$\begin{aligned}(r_2)_j^{i,\kappa} = &-\left\{\frac{(bV)_j^{i,\kappa-1} - (bV)_{j-1}^{i,\kappa-1}}{h_j} + \frac{m^i+1}{2}(fV)_{j-1/2}^{i,\kappa-1} - \left(\frac{x_{i-1/2}}{k_i} + m^i\right)(U^2)_{j-1/2}^{i,\kappa-1}\right.\\ &\left. + \frac{x_{i-1/2}}{k_i}\left(V_{j-1/2}^{i,\kappa-1} f_{j-1/2}^{i,\kappa-1} + V_{j-1/2}^{i-1} f_{j-1/2}^{i,\kappa-1} - f_{j-1/2}^{i-1} V_{j-1/2}^{i,\kappa-1}\right)\right\}\\ &-\left\{\frac{(bV)_j^{i-1} - (bV)_{j-1}^{i-1}}{h_j} + \frac{m^{i-1}+1}{2}(fV)_{j-1/2}^{i-1} + \left(\frac{x_{i-1/2}}{k_i} - m^{i-1}\right)(U^2)_{j-1/2}^{i-1}\right.\\ &\left. - \frac{x_{i-1/2}}{k_i} V_{j-1/2}^{i-1} f_{j-1/2}^{i-1} + 2m^{i-1/2}\right\}\end{aligned}$$

Together with the boundary conditions this system is repeatedly solved until the Newton iterates $\delta f_j^{i,\kappa}$, $\delta U_j^{i,\kappa}$, $\delta V_j^{i,\kappa}$ are small enough to be neglected. As frequently experienced in discretized boundary value problems the resulting set of linearized finite difference equations displays a block-tridiagonal structure which permits a fast algorithm being applied to the linear equation solution. Block-tridiagonal matrices are composed of submatrices, named blocks, of which only those residing on main and both adjacent diagonals have nonzero entries. Equations and boundary conditions of the discretized boundary layer problem require a special arrangement to exhibit this block-tridiagonal structure. The system consists of J sets, each of which include three equations:

a. First set of equations (index $j = 1$)
   1. Wall boundary condition prescribing no penetration
   2. Wall boundary condition prescribing zero tangential velocity
   3. Second auxiliary relation (linking U' and V) of the first box

b. Intermediate sets of equations (index $2 \le j \le J-1$)
   1. First auxiliary relation (linking f' and U) of the $(j-1)$-st box
   2. Momentum equation of the $(j-1)$-st box
   3. Second auxiliary relation (linking U' and V) of the j-th box

c. Last set of equations (index $j = J$)
   1. First auxiliary relation (linking f' and U) of the last box
   2. Momentum equation of the last box
   3. Edge boundary condition.

Boxes are numbered, the first referring to that at the wall, the last referring to that at the boundary layer edge. With $\{\delta_j^{i,\kappa}\} = \{\delta f_j^{i,\kappa}, \delta U_j^{i,\kappa}, \delta V_j^{i,\kappa}\}^T$ and $\{r_j^{i,\kappa}\} = \{(r_1)_j^{i,\kappa}, (r_2)_j^{i,\kappa}, (r_3)_j^{i,\kappa}\}^T$ denoting vectors of the unknown Newton iterates and the known right hand sides, respectively, the linearized system can be expressed according to

$$\begin{bmatrix} [A_1^{i,\kappa}] & [C_1^{i,\kappa}] & & & & \\ [B_2^{i,\kappa}] & [A_2^{i,\kappa}] & [C_2^{i,\kappa}] & & & \\ & \ddots & \ddots & \ddots & & \\ & [B_j^{i,\kappa}] & [A_j^{i,\kappa}] & [C_j^{i,\kappa}] & & \\ & & \ddots & \ddots & \ddots & \\ & & [B_{J-1}^{i,\kappa}] & [A_{J-1}^{i,\kappa}] & [C_{J-1}^{i,\kappa}] & \\ & & & [B_J^{i,\kappa}] & [A_J^{i,\kappa}] & \end{bmatrix} \begin{Bmatrix} \{\delta_1^{i,\kappa}\} \\ \{\delta_2^{i,\kappa}\} \\ \vdots \\ \{\delta_j^{i,\kappa}\} \\ \vdots \\ \{\delta_{J-1}^{i,\kappa}\} \\ \{\delta_J^{i,\kappa}\} \end{Bmatrix} = \begin{Bmatrix} \{r_1^{i,\kappa}\} \\ \{r_2^{i,\kappa}\} \\ \vdots \\ \{r_j^{i,\kappa}\} \\ \vdots \\ \{r_{J-1}^{i,\kappa}\} \\ \{r_J^{i,\kappa}\} \end{Bmatrix}$$

where the blocks are 3×3-matrices being defined as

$$[A_j^{i,\kappa}] = \begin{bmatrix} 1 & -h_j/2 & 0 \\ (s_3)_j^{i,\kappa} & (s_5)_j^{i,\kappa} & (s_1)_j^{i,\kappa} \\ 0 & -1 & -h_{j+1}/2 \end{bmatrix} \qquad \text{for } 2 \le j \le J-1$$

$$[B_j^{i,\kappa}] = \begin{bmatrix} -1 & -h_j/2 & 0 \\ (s_4)_j^{i,\kappa} & (s_6)_j^{i,\kappa} & (s_2)_j^{i,\kappa} \\ 0 & 0 & 0 \end{bmatrix} \qquad \text{for } 2 \le j \le J$$

$$[C_j^{i,\kappa}] = \begin{bmatrix} 0 & 0 & 0 \\ 0 & 0 & 0 \\ 0 & 1 & -h_{j+1}/2 \end{bmatrix} \qquad \text{for } 1 \le j \le J-1$$

$$[A_1^{i,\kappa}] = \begin{bmatrix} 1 & 0 & 0 \\ 0 & 1 & 0 \\ 0 & -1 & -h_2/2 \end{bmatrix}, \qquad [A_J^{i,\kappa}] = \begin{bmatrix} 1 & -h_J/2 & 0 \\ (s_3)_J^{i,\kappa} & (s_5)_J^{i,\kappa} & (s_1)_J^{i,\kappa} \\ 0 & 1 & 0 \end{bmatrix}$$

and where the right hand sides are obtained from

$$(r_1)_j^{i,\kappa} = f_{j-1}^{i,\kappa-1} - f_j^{i,\kappa-1} + h_j U_{j-1/2}^{i,\kappa-1} \qquad \text{for } 2 \le j \le J$$

$$(r_2)_j^{i,\kappa} = \begin{cases} \text{as given by} \\ \text{momentum equation} \end{cases} \qquad \text{for } 2 \le j \le J$$

$$(r_3)_j^{i,\kappa} = U_j^{i,\kappa-1} - U_{j-1}^{i,\kappa-1} + h_{j+1} V_{j+1/2}^{i,\kappa-1} \qquad \text{for } 1 \le j \le J-1$$

$$(r_1)_1^{i,\kappa} = 0, \qquad (r_2)_1^{i,\kappa} = 0, \qquad (r_3)_J^{i,\kappa} = 0$$

The variety of indices explains itself by the 2-dimensionality and nonlinear character of the problem:
1. The superscript "i" indicates the location along the blade surface.
2. The subscript "j" denotes the location perpendicular to the blade surface.
3. The superscript "κ" designates the iteration counter.

The unknowns are the Newton iterates of streamfunction and its first and second derivative at the i-th streamwise position of the κ-th iteration all across the boundary layer. The above system of linear equations can be solved most efficiently by Keller's block elimination method, which consists primarily of two types of recursions. A forward step eliminates the lower diagonal of submatrices, wheras the backward step solves the remaining system from bottom to top.

Note on discretization: The averaging of all terms is carried through such that the number of generated terms is a minimum, which turns out to be trivial for single quantities, but has some impact on the product terms. Furthermore, averaging makes no difference whether acting on dependent variables or dependent parameters like "m" and "b". Let a and d be any dependent flow quantities, then discretization is performed on the basis of the following rules:

1. Evaluation of single terms: $$a^{i-1/2}_{j-1/2} = \frac{1}{4}(a^i_j + a^i_{j-1} + a^{i-1}_j + a^{i-1}_{j-1})$$

2. Evaluation of differential quotients: $$\left(\frac{\partial a}{\partial x}\right)^{i-1/2} = \frac{a^i - a^{i-1}}{k_i}$$
$$\left(\frac{\partial a}{\partial \eta}\right)_{j-1/2} = \frac{a_j - a_{j-1}}{h_j}$$

3. Evaluation of product terms: $$(ad)_{j-1/2} = \frac{1}{2}[(ad)_j + (ad)_{j-1}] = \frac{1}{2}(a_j d_j + a_{j-1} d_{j-1})$$

rather than: $$(ad)_{j-1/2} = \frac{1}{4}(a_j d_j + a_j d_{j-1} + a_{j-1} d_j + a_{j-1} d_{j-1})$$

Although the second way of evaluating the product term is just as valid as the first one, the more straightforward fashion of the first formula is preferred throughout the method. Care is advised in the reverse process, so $a_{j-1/2}\, d_{j-1/2} \neq (ad)_{j-1/2}$ because of the above agreement.

3.2 Interactive boundary layer method

The integration of boundary layer equations subject to an imposed pressure distribution terminates at the point of zero skin friction. Moreover, direct methods are restricted to weakly interacting regions, where viscous disturbances to the inviscid flow remain small. Strong interaction arises for example from boundary layer separation or the rapid flow acceleration downstream of the trailing edge, both of which cause substantial changes in the external velocity distribution due to viscous displacement. Interactive methods are designed to permit integration through the point of zero skin friction and to account for strong interaction. The boundary layer approach is maintained in strongly interacting regions, but accommodations apply to the status of external velocity and edge boundary condition. In contrast to direct and inverse methods both external velocity and displacement thickness are treated here as unknown quantities, reflecting the elliptic character of the outer flow. This introduces apparently one additional unknown into the viscous flow problem, whose solution can be achieved either by an eigenvalue method or the Mechul function method, the latter of which being preferred here. The edge boundary condition of the direct problem is supplemented by the so-called interactive boundary condition, which relates the unknown external velocity with its inviscid and "displacement-perturbation-related" contributions. Boundary layer equations in the following form constitute a system in the unknown functions $u(x, y)$, $v(x, y)$, and $u_e(x, y)$

$$\frac{\partial u}{\partial x} + \frac{\partial v}{\partial y} = 0$$
$$u\frac{\partial u}{\partial x} + v\frac{\partial u}{\partial y} = u_e\frac{\partial u_e}{\partial x} + \nu\frac{\partial}{\partial y}(b\frac{\partial u}{\partial y})$$
$$0 = \frac{\partial u_e}{\partial y}$$

The system consists of continuity equation, x-momentum equation, and the seemingly unnecessary y-momentum equation, wherein pressure in the momentum equations has been expressed in terms of the external velocity. The Mechul function approach assumes that the external velocity be a function of two arguments, resulting in the need for the trivial y-momentum equation. The reason for considering $u_e(x, y)$ rather than $u_e(x)$ is of a purely numerical nature, i.e., such a provision allows an easy setup of finite difference equations, avoiding nonlinear eigenvalue techniques. The governing equations are complemented by proper boundary conditions: The velocity components u and v are required to satisfy the no-slip condition at the

surface of the blade and the horizontal component must merge smoothly into the outer flow at the boundary layer edge

$$y = 0: \qquad u(x,0) = 0, \quad v(x,0) = 0$$

$$y = y_e: \qquad u(x,y_e) = u_e(x,y_e), \quad u_e(x,y_e) = u_{ef}(x) + \frac{1}{\pi}\int \frac{d}{d\xi}(u_e\delta^*)\frac{d\xi}{x-\xi}$$

with $u_{ef}(x)$ denoting the inviscid velocity distribution and the second term, named Hilbert integral, approximating the perturbation velocity due to viscous effects.

Interactive methods can be employed in both attached and separated flow regions ,while direct methods cannot do so because of their breakdown related to the Goldstein singularity, nor inverse methods because of their poor convergence rates. Since interactive methods offer such a favourable behaviour, they are used in the current scheme for the main parts of the blade. Only the stagnation point singularity prohibits an exclusive use of the interactive method. The steps which turn the partial differential equations of the interactive problem into a linear system of algebraic equations resemble those of the direct method so that only major steps and their results will be repeated here. After the introduction of a streamfunction ($u = \partial\psi/\partial y$ and $v = -\partial\psi/\partial x$), the equations undergo a transformation, which scales the normal coordinate y. streamfunction ψ, and the external velocity u_e with reference to a constant velocity u_0 and the local streamwise coordinate x

$$\eta = \sqrt{\frac{u_0}{\nu x}}\, y$$

$$f(x,\eta) = \frac{1}{\sqrt{u_0 \nu x}}\,\psi(x,y)$$

$$\bar{W}(x,\eta) = \frac{u_e(x,y)}{u_0}$$

where u_0 is taken as the magnitude of vector mean velocity. The concept of constant boundary layer thickness. attained by Falkner-Skan variables (with u_e as reference velocity), has to be abandoned because the external velocity is unknown in interactive calculations. However. provided that the integration does not start in the immediate neighbourhood of the stagnation point. growth of the boundary layer thickness can be kept limited. In terms of these so-called semi-transformed coordinates equations ,written as a first order system by means of two additional dependent variables U and V, and boundary conditions take the form

$$f' = U$$

$$U' = V$$

$$(bV)' + \frac{1}{2} fV + x\bar{W}\frac{\partial \bar{W}}{\partial x} = x\left(U\frac{\partial U}{\partial x} - V\frac{\partial f}{\partial x}\right)$$

$$\bar{W}' = 0$$

$$\eta = 0: \qquad U(x,0) = 0, \quad f(x,0) = 0$$

$$\eta = \eta_e: \qquad U(x,\eta_e) = \bar{W}(x,\eta_e)$$

$$\bar{W}(x,\eta_e) = \frac{u_{ef}(x)}{u_0} + \frac{1}{\pi}\int \frac{d}{d\xi}\left\{\sqrt{\frac{\nu\xi}{u_0}}\left[\bar{W}(\xi,\eta_e)\,\eta_e - f(\xi,\eta_e)\right]\right\}\frac{d\xi}{x-\xi}$$

The discretization of the flowfield follows closely the above outlined procedure of the direct method. covering the generation of an orthogonal grid and the introduction of central differences and two-point-averages. The overall solution proceeds in the downstream direction. accounting for downstream travelling disturbances only. In regions of backflow disturbances propagate against the direction of integration causing numerical instabilities. On the assumption that backflow velocities are comparatively small. a stable integration can be carried out by adopting the Flare approximation (Flugge-Lotz and Reyhner). in which the streamwise convection term $u\partial u/\partial x$ is set equal to zero in regions of backflow. With

$$\vartheta^i_{j-1/2} = \begin{cases} 1 & \text{if } U^i_{j-1/2} \geq 0 \\ 0 & \text{if } U^i_{j-1/2} < 0 \end{cases}$$

designating an "on-off-switch" of the streamwise convection term, the finite difference equations of the interactive boundary layer problem become

$$\frac{f_j^i - f_{j-1}^i}{h_j} = \frac{1}{2}(U_j^i + U_{j-1}^i)$$

$$\frac{U_j^i - U_{j-1}^i}{h_j} = \frac{1}{2}(V_j^i + V_{j-1}^i)$$

$$\frac{(bV)_j^{i-1/2} - (bV)_{j-1}^{i-1/2}}{h_j} + \frac{1}{2}(fV)_{j-1/2}^{i-1/2} + x_{i-1/2}\left(W^{i-1/2}\,\frac{W^i - W^{i-1}}{k_i}\right)_{j-1/2}$$

$$= x_{i-1/2}\left[\vartheta_{j-1/2}^i\left(U^{i-1/2}\,\frac{U^i - U^{i-1}}{k_i}\right)_{j-1/2} - \left(V^{i-1/2}\,\frac{f^i - f^{i-1}}{k_i}\right)_{j-1/2}\right]$$

$$\frac{W_j^i - W_{j-1}^i}{h_j} = 0$$

Boundary conditions are expressed in terms of nodal values ,too, whereby the evaluation of the integral occuring in the interactive boundary condition involves an approximation in the fashion of the panel method approach, leading to

$$U_1^i = 0, \qquad f_1^i = 0$$

$$U_J^i = W_J^i, \qquad W_J^i = \tilde{g}_i + \tilde{c}_{ii}(W_J^i\,\eta_J - f_J^i)$$

where $\tilde{g}_i$ and $\tilde{c}_{ii}$ denote a parameter and the diagonal element of the interaction matrix, resulting from a discrete approximation to the Hilbert integral. Averaging as well as centering is supposed to obey the principle that the number of generated terms approaches a minimum. This entails ordinary differential equations, like the y-momentum equation, being centered about the middle of the downstream face and partial differential equations, like the x-momentum equation, being centered about the middle of the box.

A balance of unknowns, which occur here as vectors in four components, $\{f_j^i, U_j^i, V_j^i, W_j^i\}^T$, confirms the principal solvability of the system: The J quadruplets of unknowns match with a total of $4J$ equations, including $2(J-1)$ auxiliary relations, $(J-1)$ x-momentum and $(J-1)$ y-momentum equations, each of which corresponding to one of the $(J-1)$ net rectangles, and 4 boundary conditions. After linearizing this system around the values of the preceding iteration (iteration counter "$\kappa-1$"), respectively around the solution of the adjacent upstream x-station in case of the first iteration, we arrive at a linear system in the Newton iterates $\delta f_j^{i,\kappa}, \delta U_j^{i,\kappa}, \delta V_j^{i,\kappa}, \delta W_j^{i,\kappa}$

$$\delta f_j^{i,\kappa} - \delta f_{j-1}^{i,\kappa} - \frac{h_j}{2}(\delta U_j^{i,\kappa} + \delta U_{j-1}^{i,\kappa}) = f_{j-1}^{i,\kappa-1} - f_j^{i,\kappa-1} + h_j U_{j-1/2}^{i,\kappa-1}$$

$$\delta U_j^{i,\kappa} - \delta U_{j-1}^{i,\kappa} - \frac{h_j}{2}(\delta V_j^{i,\kappa} + \delta V_{j-1}^{i,\kappa}) = U_{j-1}^{i,\kappa-1} - U_j^{i,\kappa-1} + h_j V_{j-1/2}^{i,\kappa-1}$$

$$(s_1)_j^{i,\kappa}\delta V_j^{i,\kappa} + (s_2)_j^{i,\kappa}\delta V_{j-1}^{i,\kappa} + (s_3)_j^{i,\kappa}\delta f_j^{i,\kappa} + (s_4)_j^{i,\kappa}\delta f_{j-1}^{i,\kappa} + (s_5)_j^{i,\kappa}\delta U_j^{i,\kappa} + (s_6)_j^{i,\kappa}\delta U_{j-1}^{i,\kappa}$$
$$+ (s_7)_j^{i,\kappa}\delta W_j^{i,\kappa} + (s_8)_j^{i,\kappa}\delta W_{j-1}^{i,\kappa} = (r_2)_j^{i,\kappa}$$

$$\delta W_j^{i,\kappa} - \delta W_{j-1}^{i,\kappa} = W_{j-1}^{i,\kappa-1} - W_j^{i,\kappa-1}$$

supplemented by the two components of no-slip condition, edge and interactive boundary condition

$$\delta U_1^{i,\kappa} = 0, \quad \delta f_1^{i,\kappa} = 0$$

$$\delta U_J^{i,\kappa} - \delta W_J^{i,\kappa} = 0$$

$$\delta f_J^{i,\kappa} + \left(\frac{1}{\tilde{c}_{ii}} - \eta_J\right)\delta W_J^{i,\kappa} = \frac{\tilde{g}_i}{\tilde{c}_{ii}} - f_J^{i,\kappa-1} - \left(\frac{1}{\tilde{c}_{ii}} - \eta_J\right)W_J^{i,\kappa-1}$$

Terms have been grouped such that known quantities reside on the right hand sides, while unknown quantities appear left of the equal sign. The abbreviated coefficients in the momentum equation are defined by

$$(s_1)_j^{i,\kappa} = \frac{b_j^{i,\kappa-1}}{h_j} + \frac{x_{i-1/2}}{2k_i}\left(f_{j-1/2}^{i,\kappa-1} - f_{j-1/2}^{i-1}\right) + \frac{1}{4} f_j^{i,\kappa-1}$$

$$(s_2)_j^{i,\kappa} = -\frac{b_j^{i,\kappa-1}}{h_j} + \frac{x_{i-1/2}}{2k_i}\left(f_{j-1/2}^{i,\kappa-1} - f_{j-1/2}^{i-1}\right) + \frac{1}{4} f_{j-1}^{i,\kappa-1}$$

$$(s_3)_j^{i,\kappa} = \frac{x_{i-1/2}}{2k_i}\left(V_{j-1/2}^{i,\kappa-1} + V_{j-1/2}^{i-1}\right) + \frac{1}{4} V_j^{i,\kappa-1}$$

$$(s_4)_j^{i,\kappa} = \frac{x_{i-1/2}}{2k_i}\left(V_{j-1/2}^{i,\kappa-1} + V_{j-1/2}^{i-1}\right) + \frac{1}{4} V_{j-1}^{i,\kappa-1}$$

$$(s_5)_j^{i,\kappa} = -\frac{x_{i-1/2}}{k_i} U_j^{i,\kappa-1}\vartheta_{j-1/2}^{i}$$

$$(s_6)_j^{i,\kappa} = -\frac{x_{i-1/2}}{k_i} U_{j-1}^{i,\kappa-1}\vartheta_{j-1/2}^{i}$$

$$(s_7)_j^{i,\kappa} = \frac{x_{i-1/2}}{k_i} W_j^{i,\kappa-1}$$

$$(s_8)_j^{i,\kappa} = \frac{x_{i-1/2}}{k_i} W_{j-1}^{i,\kappa-1}$$

and the right hand side of the very equation reads

$$(r_2)_j^{i,\kappa} = -\left\{ \frac{(bV)_j^{i,\kappa-1} - (bV)_{j-1}^{i,\kappa-1}}{h_j} + \frac{1}{2}(fV)_{j-1/2}^{i,\kappa-1} \right.$$
$$\left. + \frac{x_{i-1/2}}{k_i}\left[(W^2)_{j-1/2}^{i,\kappa-1} - (U^2)_{j-1/2}^{i,\kappa-1}\vartheta_{j-1/2}^{i} + V_{j-1/2}^{i,\kappa-1} f_{j-1/2}^{i,\kappa-1} + V_{j-1/2}^{i-1} f_{j-1/2}^{i,\kappa-1} - f_{j-1/2}^{i-1} V_{j-1/2}^{i,\kappa-1} \right] \right\}$$
$$- \left\{ \frac{(bV)_j^{i-1} - (bV)_{j-1}^{i-1}}{h_j} + \frac{1}{2}(fV)_{j-1/2}^{i-1} - \frac{x_{i-1/2}}{k_i}\left[(W^2)_{j-1/2}^{i-1} - (U^2)_{j-1/2}^{i-1}\vartheta_{j-1/2}^{i} + V_{j-1/2}^{i-1} f_{j-1/2}^{i-1} \right] \right\}$$

Since the overall procedure involves a repetitive linear pattern to approach the solution of the nonlinear system, the linear equation solver has to be as fast as possible. Fast algorithms take advantage of specific matrix structures, one of which is the block-tridiagonal structure, which can be enforced in this method by the following arrangement of equations and boundary conditions:

a. First set of equations (index $j = 1$)
   1. Wall boundary condition prescribing no penetration
   2. Wall boundary condition prescribing zero tangential velocity
   3. Second auxiliary relation (linking U' and V) of the first box
   4. Trivial y-momentum equation of the first box first box

b. Intermediate sets of equations (index $2 \leq j \leq J-1$)
   1. First auxiliary relation (linking f' and U) of the $(j-1)$-st box
   2. Momentum equation of the $(j-1)$-st box
   3. Second auxiliary relation (linking U' and V) of the
   4. Trivial y-momentum equation of the j-th box j-th box

c. Last set of equations (index $j = J$)
   1. First auxiliary relation (linking f' and U) of the last box
   2. Momentum equation of the last box
   3. Interactive boundary condition
   4. Edge boundary condition.

Following these instructions equations and boundary conditions can be summarized in matrix-vector form, offering the desired structure

$$\begin{bmatrix} [A_1^{i,\kappa}] & [C_1^{i,\kappa}] & & & & \\ [B_2^{i,\kappa}] & [A_2^{i,\kappa}] & [C_2^{i,\kappa}] & & & \\ & \ddots & \ddots & \ddots & & \\ & [B_j^{i,\kappa}] & [A_j^{i,\kappa}] & [C_j^{i,\kappa}] & & \\ & & \ddots & \ddots & \ddots & \\ & & [B_{J-1}^{i,\kappa}] & [A_{J-1}^{i,\kappa}] & [C_{J-1}^{i,\kappa}] & \\ & & & [B_J^{i,\kappa}] & [A_J^{i,\kappa}] \end{bmatrix} \begin{Bmatrix} \{\delta_1^{i,\kappa}\} \\ \{\delta_2^{i,\kappa}\} \\ \vdots \\ \{\delta_j^{i,\kappa}\} \\ \vdots \\ \{\delta_{J-1}^{i,\kappa}\} \\ \{\delta_J^{i,\kappa}\} \end{Bmatrix} = \begin{Bmatrix} \{r_1^{i,\kappa}\} \\ \{r_2^{i,\kappa}\} \\ \vdots \\ \{r_j^{i,\kappa}\} \\ \vdots \\ \{r_{J-1}^{i,\kappa}\} \\ \{r_J^{i,\kappa}\} \end{Bmatrix}$$

where $\{\delta_j^{i,\kappa}\} = \{\delta f_j^{i,\kappa}, \delta U_j^{i,\kappa}, \delta V_j^{i,\kappa}, \delta W_j^{i,\kappa}\}^T$ and $\{r_j^{i,\kappa}\} = \{(r_1)_j^{i,\kappa}, (r_2)_j^{i,\kappa}, (r_3)_j^{i,\kappa}, (r_4)_j^{i,\kappa}\}^T$ denote four dimensional vectors of the unknown Newton iterates and the known right hand sides. respectively. The blocks in the three diagonals of the above matrix have the dimension 4×4 and can be obtained from

$$[A_j^{i,\kappa}] = \begin{bmatrix} 1 & -h_j/2 & 0 & 0 \\ (s_3)_j^{i,\kappa} & (s_5)_j^{i,\kappa} & (s_1)_j^{i,\kappa} & (s_7)_j^{i,\kappa} \\ 0 & -1 & -h_{j+1}/2 & 0 \\ 0 & 0 & 0 & -1 \end{bmatrix} \qquad \text{for } 2 \le j \le J-1$$

$$[B_j^{i,\kappa}] = \begin{bmatrix} -1 & -h_j/2 & 0 & 0 \\ (s_4)_j^{i,\kappa} & (s_6)_j^{i,\kappa} & (s_2)_j^{i,\kappa} & (s_8)_j^{i,\kappa} \\ 0 & 0 & 0 & 0 \\ 0 & 0 & 0 & 0 \end{bmatrix} \qquad \text{for } 2 \le j \le J$$

$$[C_j^{i,\kappa}] = \begin{bmatrix} 0 & 0 & 0 & 0 \\ 0 & 0 & 0 & 0 \\ 0 & 1 & -h_{j+1}/2 & 0 \\ 0 & 0 & 0 & 1 \end{bmatrix} \qquad \text{for } 1 \le j \le J-1$$

$$[A_1^{i,\kappa}] = \begin{bmatrix} 1 & 0 & 0 & 0 \\ 0 & 1 & 0 & 0 \\ 0 & -1 & -h_2/2 & 0 \\ 0 & 0 & 0 & -1 \end{bmatrix}, \qquad [A_J^{i,\kappa}] = \begin{bmatrix} 1 & -h_J/2 & 0 & 0 \\ (s_3)_J^{i,\kappa} & (s_5)_J^{i,\kappa} & (s_1)_J^{i,\kappa} & (s_7)_j^{i,\kappa} \\ 1 & 0 & 0 & 1/\tilde{c}_{ii} - \eta_J \\ 0 & 1 & 0 & -1 \end{bmatrix}$$

The components of the right hand side vectors can be calculated from the following formulae

$$(r_1)_j^{i,\kappa} = f_{j-1}^{i,\kappa-1} - f_j^{i,\kappa-1} + h_j U_{j-1/2}^{i,\kappa-1} \qquad \text{for } 2 \le j \le J$$

$$(r_2)_j^{i,\kappa} = \begin{cases} \text{as given by} \\ \text{momentum equation} \end{cases} \qquad \text{for } 2 \le j \le J$$

$$(r_3)_j^{i,\kappa} = U_j^{i,\kappa-1} - U_{j-1}^{i,\kappa-1} + h_{j+1} V_{j+1/2}^{i,\kappa-1} \qquad \text{for } 1 \le j \le J-1$$

$$(r_4)_j^{i,\kappa} = \Pi_j^{i,\kappa-1} - \Pi_{j+1}^{i,\kappa-1} \qquad \text{for } 1 \le j \le J-1$$

$$(r_1)_1^{i,\kappa} = 0, \qquad (r_2)_1^{i,\kappa} = 0, \qquad (r_3)_J^{i,\kappa} = \frac{\tilde{g}_i - \tilde{c}_{ii} f_J^{i,\kappa-1} - (1 - \tilde{c}_{ii}\eta_J)\Pi_J^{i,\kappa-1}}{\tilde{c}_{ii}}, \qquad (r_4)_J^{i,\kappa} = 0$$

The numerical solution of the above system can again be achieved by Keller's block elimination method. which works very much like a Gauss's algorithm. but .firstly. matrices are eliminated instead of scalars. and. secondly. quite a few manipulations can be saved because of sparse occupation.

3.3 Interaction model

The coupling of the boundary layer and external inviscid flow is referred to as interaction model. Basically, the interaction consists of thickening the effective blade shape by viscous displacement. which in turn causes changes in the surface pressure. The exchange of information between viscous and inviscid regions takes place via the boundary conditions only, which is the specification of either an impermeable displacement surface or a nonzero wall transpiration at the original surface in case of inviscid flow, respectively the prescription of either pressure, or displacement thickness, or a linear combination of both in case of viscous flow. The interaction is called weak if viscous effects on pressure remain small. while situations where viscous disturbances to the inviscid flow field are substantial demand the application of strong simultaneous interaction. Interaction models fall into four types, the first three of which provide loose coupling of viscous and inviscid regions:

1. The direct interaction method combines a direct inviscid and a direct viscous flow solver. This classical approach achieves a solution by iterative matching of boundary layer calculations with prescribed pressure and inviscid calculations with prescibed displacement thickness. The alternate treatment of pressure and displacement thickness leads to a local breakdown of the procedure when slight changes in pressure entail significant changes in displacement thickness.
2. In inverse methods the roles of displacement thickness and pressure are interchanged. Hence the inviscid flow equations determine the displacement thickness distribution, which is imposed as boundary condition on the viscous flow calculation. The results of which is the pessure, which closes the cycle by being input to the inviscid flow computation. The hierarchical manner of solving the complete flow problem excludes this model just as the previous one from handling strongly interacting regions.
3. The semi-inverse interaction method is composed of a direct inviscid and an inverse viscous flow solver. Both parts of the scheme process the same input, i.e. displacement thickness. and generate the same output. i.e. pressure. After each cycle an updated displacement thickness is relaxed based on the deviation of the two pressure distributions. which should coincide upon convergence.

The existence of a definite hierarchy between boundary layer and outer flow in the above mentioned methods gives rise to a limited rate of feedback between both regions. Strong interaction models incorporate the outer flow somehow in the boundary layer calculations. for example by the following interaction law:

4. Simultaneous (or strong) interaction methods solve the boundary layer equations subject to an interaction law as outer boundary condition. which retrieves the elliptic character of the outer flow. No definite assignment of displacement thickness and pressure can be made to viscous and inviscid region. Rather. both quantities are treated as unknowns. related by the interaction law. The procedure emphasizes simultaneous solution for both displacement thickness and pressure.

In the following the currently used interaction law will be formulated in terms of displacement thickness and external velocity. the latter being related to pressure by Bernoulli's equation. Both inviscid external velocity. resulting from a potential flow calculation around the original blade, u_{eI}, and a correction term due to viscous displacement, $u_{e\delta}$, are assumed to contribute to the total external velocity

$$u_e(x) = u_{eI}(x) + u_{e\delta}(x)$$

The contribution due to viscous effects can be evaluated by means of the blowing velocity concept. which has its origin in a paper by Lighthill [16]. He proved that the effect of boundary layers on the outer flow can be represented by a surface distribution of sources. Nonzero normal velocities at the surface of blades. being induced by this very source distribution. are intended to displace streamlines from the surface such that the virtual displacement surface becomes a streamline (see figure 4 on page 12)

$$\frac{d\delta^*(x)}{dx} = \frac{v(x,\delta^*)}{u_e(x)}$$

where $v(x,\delta^*)$ denotes the vertical velocity component on the displacement surface. Since it is sufficient to approximate the correction term $u_{e\delta}$. further deductions make use of the thin airfoil approach. Firstly. streamwise upper and lower surfaces of the blade will be considered flat plates in this context. implying that the blowing velocity equals half the local source strength. and ,secondly. the displacement thickness is

supposed to be so small that the horizontal velocity components of the inviscid flow do not vary across the boundary layer

$$\frac{\sigma(x)}{2} = v(x,0) = v(x,\delta^*) - \int_0^{\delta^*} \frac{\partial v}{\partial y}\, dy = \frac{d}{dx}(u_e \delta^*)$$

Unlike vertical components horizontal velocities are affected by all sources distributed along the supposedly flat surface. Eventually the viscous correction term is given by the well known thin airfoil integral, which is referred to here as Hilbert integral

$$u_{e\delta}(x) = \frac{1}{2\pi} \int_{x_b}^{x_e} \frac{\sigma(\xi)}{x-\xi}\, d\xi = \frac{1}{\pi} \int_{x_b}^{x_e} \frac{d}{d\xi}(u_e \delta^*)\, \frac{d\xi}{x-\xi}$$

As indicated by the integration limits interaction is restricted to a finite region $x_b \le x \le x_e$ on either streamwise upper or lower surface. The numerical implementation of the interaction law requires some discrete approximation of the above thin airfoil integral. Adopting the panel method approach, which concerns here a piecewise approximation of the continuous blowing velocity $d(u_e\delta^*)/dx$ to allow piecewise analytical integration, the integral can be written as a finite series

$$\frac{1}{\pi} \int_{x_b}^{x_e} \frac{d}{d\xi}(u_e \delta^*)\, \frac{d\xi}{x-\xi} = \sum_{k=1}^{K} c_{ik} (u_e \delta^*)^k$$

with $[c_{ik}]$ denoting a matrix of interaction coefficients. Recalling that the boundary layer calculation at a streamwise position involves iterations, the inviscid contribution can be included in the total external velocity of the previous Newton iteration (identified by "$\kappa-1$"), leading to a generalized version of the interaction law

$$(u_e)^{i,\kappa} = (u_e)^{i,\kappa-1} + \sum_{k=1}^{K} c_{ik} \left[(u_e\delta^*)^{k,\kappa} - (u_e\delta^*)^{k,\kappa-1} \right]$$

Since displacement thickness does not belong to the dependent variables, $(\delta^*)^{i,\kappa}$, the displacement thickness of the streamwise position currently being solved, must be expressed in terms of dependent variables to make allowance for its unknown status. With $(\delta^*)^{i,\kappa}$ being replaced by $y_J - \psi_J^{i,\kappa}/(u_e)^{i,\kappa}$ and after separating known and unknown terms, the interaction law takes its almost final form

$$(u_e)^{i,\kappa}(1 - c_{ii}\, y_J) + c_{ii}\, \psi_J^{i,\kappa} = g_i^{\kappa}$$

with

$$g_i^{\kappa} = (u_e)^{i,\kappa-1} + \sum_{\substack{k=1 \\ k\neq i}}^{K} c_{ik} \left[(u_e\delta^*)^{k,\kappa} - (u_e\delta^*)^{k,\kappa-1} \right] - c_{ii} (u_e y_J - \psi_J)^{i,\kappa-1}$$

Implementing this relation necessitates a known right hand side, which can be evaluated only in an approximate fashion, because the terms $(u_e\delta^*)^{k,\kappa}$ are not known yet downstream of the current x-location. To ensure interaction also over this region, these terms are taken from the previous iteration updated by some relaxation formula. With $\tilde{c}_{ik} = c_{ik}\sqrt{\nu x/u_0}$ and $\tilde{g}_i^{\kappa} = g_i^{\kappa}/u_0$ designating dimensionless interaction coefficients and right hand side, respectively, the actually coded interaction law can be written in terms of semi-transformed coordinates

$$W_J^{i,\kappa}(1 - \tilde{c}_{ii}\, \eta_J) + \tilde{c}_{ii}\, f_J^{i,\kappa} = \tilde{g}_i^{\kappa}$$

This equation, being used as an outer boundary condition in the viscous flow computation, relates the unknown external velocity and the unknown displacement thickness of the i-th boundary layer station, whereby displacement thickness has been expressed by streamfunction and external velocity. Because of the elliptic character of the outer flow, which has been incorporated in the boundary layer via the interaction law, solution requires a global iteration, consisting of several viscous sweeps to be performed over both the streamwise upper and lower surface.

Note on the calculation of interaction coefficients: Let the continuous function "external velocity times displacement thickness", denoted by D, be discretized at a finite number of streamwise positions. The thin airfoil integral then can be approximated by a finite series of weighted "D's" at the very locations

$$\frac{1}{\pi}\int_{x_1}^{x_K}\frac{dD}{d\xi}\,\frac{d\xi}{x_i-\xi}=\sum_{k=1}^{K}c_{ik}\,D_k$$

The weights are the interaction coefficients c_{ik}, with the first subscript indicating the streamwise position, where the correction term $u_{e\delta}$ is to be evaluated, and the second indicating the location, whose effect is accounted for. With a properly interpolated D-function, integration can be carried out analytically piece by piece. Provided the point under consideration does not fall within the limits of integration. D will be interpolated linearly. Piecewise linear functions can be built up by overlapping triangular distributions, integration over which yields the coefficients whose $k\neq i$, $k\neq i-1$, $k\neq i+1$

$$c_{ik}=\frac{1}{\pi D_k}\int_{x_{k-1}}^{x_{k+1}}\frac{dD}{d\xi}\,\frac{d\xi}{x_i-\xi}\qquad\text{with}\qquad\frac{dD}{d\xi}=\begin{cases}\dfrac{D_k}{x_k-x_{k-1}} & \text{for}\quad x_{k-1}\le\xi\le x_k\\[2ex] -\dfrac{D_k}{x_{k+1}-x_k} & \text{for}\quad x_k\le\xi\le x_{k+1}\end{cases}$$

$$c_{ik}=\frac{1}{\pi}\left[\frac{1}{x_k-x_{k-1}}\ln\left|\frac{x_i-x_{k-1}}{x_i-x_k}\right|-\frac{1}{x_{k+1}-x_k}\ln\left|\frac{x_i-x_k}{x_i-x_{k+1}}\right|\right]$$

A linearly interpolated D-function would lead to singular integrals for the coefficients $k=1$, $k=i-1$, and $k=i+1$. Therefore D will be approximated by a polynomial of degree 2 in the interval $x_{i-1}\le\xi\le x_{i+1}$. Splitting again into overlapping distributions, which this time are parabolic, and applying Cauchy's principal value technique permits integration of singular integrands:
The coefficient at the middle of the inducing source distribution is given by

$$c_{ii}=\frac{1}{\pi D_i}\int_{x_{i-1}}^{x_{i+1}}\frac{dD}{d\xi}\,\frac{d\xi}{x_i-\xi}$$

$$\text{with}\quad\frac{dD}{d\xi}=\frac{D_i}{x_{i+1}-x_{i-1}}\left[\frac{x_{i+1}-x_i}{x_i-x_{i-1}}-\frac{x_i-x_{i-1}}{x_{i+1}-x_i}\right]-\frac{2(\xi-x_i)}{x_{i+1}-x_{i-1}}\left[\frac{D_i}{x_{i+1}-x_i}+\frac{D_i}{x_i-x_{i-1}}\right]$$

$$c_{ii}=\frac{1}{\pi}\left\{\left[\frac{x_{i+1}-x_i}{x_i-x_{i-1}}-\frac{x_i-x_{i-1}}{x_{i+1}-x_i}\right]\frac{1}{x_{i+1}-x_{i-1}}\ln\left|\frac{x_i-x_{i-1}}{x_i-x_{i+1}}\right|+\frac{2}{x_i-x_{i-1}}+\frac{2}{x_{i+1}-x_i}\right\}$$

The coefficient at the right of the inducing source distribution is given by

$$c_{i,i-1}=\frac{1}{\pi D_{i-1}}\int_{x_{i-2}}^{x_{i+1}}\frac{dD}{d\xi}\,\frac{d\xi}{x_i-\xi}$$

$$\text{with}\quad\frac{dD}{d\xi}=\begin{cases}\dfrac{D_{i-1}}{x_{i-1}-x_{i-2}} & \text{for}\quad x_{i-2}\le\xi\le x_{i-1}\\[2ex] -\dfrac{D_{i-1}}{x_i-x_{i-1}}\,\dfrac{x_{i+1}-x_i}{x_{i+1}-x_{i-1}}+\dfrac{2(\xi-x_i)}{x_{i+1}-x_{i-1}}\,\dfrac{D_{i-1}}{x_i-x_{i-1}} & \text{for}\quad x_{i-1}\le\xi\le x_{i+1}\end{cases}$$

$$c_{i,i-1}=\frac{1}{\pi}\left[\frac{1}{x_{i-1}-x_{i-2}}\ln\left|\frac{x_i-x_{i-2}}{x_i-x_{i-1}}\right|-\frac{x_{i+1}-x_i}{(x_i-x_{i-1})(x_{i+1}-x_{i-1})}\ln\left|\frac{x_i-x_{i-1}}{x_i-x_{i+1}}\right|-\frac{2}{x_i-x_{i-1}}\right]$$

The coefficient at the left of the inducing source distribution is given by

$$c_{i,i+1}=\frac{1}{\pi D_{i+1}}\int_{x_{i-1}}^{x_{i+2}}\frac{dD}{d\xi}\,\frac{d\xi}{x_i-\xi}$$

$$\text{with}\quad\frac{dD}{d\xi}=\begin{cases}\dfrac{D_{i+1}}{x_{i+1}-x_i}\,\dfrac{x_i-x_{i-1}}{x_{i+1}-x_{i-1}}+\dfrac{2(\xi-x_i)}{x_{i+1}-x_{i-1}}\,\dfrac{D_{i+1}}{x_{i+1}-x_i} & \text{for}\quad x_{i-1}\le\xi\le x_{i+1}\\[2ex] -\dfrac{D_{i+1}}{x_{i+2}-x_{i+1}} & \text{for}\quad x_{i+1}\le\xi\le x_{i+2}\end{cases}$$

$$c_{i,i+1}=\frac{1}{\pi}\left[\frac{x_i-x_{i-1}}{(x_{i+1}-x_i)(x_{i+1}-x_{i-1})}\ln\left|\frac{x_i-x_{i-1}}{x_i-x_{i+1}}\right|-\frac{2}{x_{i+1}-x_i}-\frac{1}{x_{i+2}-x_{i+1}}\ln\left|\frac{x_i-x_{i+1}}{x_i-x_{i+2}}\right|\right]$$

As indicated above, the overall solution is approached in an iterative process, in which alternately viscous and inviscid flow equations are being solved (see also figure 1 on page 4):

1. Calculate the external velocity distribution u_{ef} in an inviscid flow field by means of the panel method. To account for the blade-thickening due to viscous displacement, specify a nonzero normal velocity (blowing velocity) at the blade's surface.
2. March through the boundary layers of both streamwise upper and lower surface using (over the main part of the blade) the interaction law as outer boundary condition.
3. Check convergence and quit if the criterion is satisfied.
4. If the convergence criterion is not met, prepare for another cycle. Update the product-term "external velocity times displacement thickness" on the basis of the deviation between inviscid and viscous external velocity distribution

$$(u_e\delta^*)^{i,\lambda+1} = (u_e\delta^*)^{i,\lambda}\left[1+\omega\left(\frac{(u_e)^{i,\lambda}}{(u_{ef})^{i,\lambda}}-1\right)\right]$$

where λ denotes the counter of global iterations. Further, compute the blowing velocity distribution, which serves as boundary condition for the inviscid flow solution

$$(V_{wtr})^i = \frac{d}{dx}(u_e\delta^*)^{i,\lambda+1}$$

and proceed with the first step.

3.4 Turbulence modelling

The presence of additional unknown shear stresses in turbulent flows requires modelling assumptions to balance the number of unknowns and equations. Eddy viscosity models, one of which is used in the present method, relate turbulent shear stresses to mean flow quantities on an empirical basis. They draw their versatility from the convenience of maintaining the same approach and numerical formulation for both laminar and turbulent flows. The currently employed model features a zero equation closure, which presumes that the length scale can be specified by an algebraic equation. The turbulent kinematic viscosity is defined by two separate formulae, one for the inner region being based on Van Driest's approach [21], and the other for the outer region being based on a velocity defect approach

$$\nu_t = \begin{cases} \left\{0.4\,y\left[1-\exp\left(-\frac{y}{A}\right)\right]\right\}^2 \left|\frac{\partial u}{\partial y}\right| \gamma_{tr} & \text{for} \quad 0 \le y \le y_c \\ \alpha \int_0^\infty (u_e - u)\,dy\;\gamma_{tr}\,\gamma & \text{for} \quad y_c \le y \le \delta \end{cases}$$

$$\text{where} \quad A = 26\nu \Big/ \left(\nu\frac{\partial u}{\partial y}\right)^{1/2}_{max} \quad \text{and} \quad \gamma = \frac{1}{1+5.5\,(y/\delta)^6}$$

Continuity of the turbulent kinematic viscosities is established by defining y_c as the distance from the wall where expressions for inner and outer region do agree. Since transition is not an instantaneous process, an intermediate status of flow, called transitional flow, is assumed between the laminar and fully turbulent regions. This region is taken into account by introduction of an intermittency factor, which smears out the step-shaped change from kinematic to eddy viscosity

$$\gamma_{tr} = 1 - \exp\left[-\frac{u_e^3}{G_{\gamma_{tr}}\nu^2}\,R_{x_{tr}}^{-1.34}\,(x-x_{tr})\int_{x_{tr}}^{x}\frac{d\xi}{u_e}\right]$$

where $R_{x_{tr}}$ denotes the Reynolds number based on external velocity and streamwise location x_{tr} at onset of transition. A value of 1200 was originally assigned to the empirical constant $G_{\gamma_{tr}}$. However, numerical experiments seem to indicate that low Reynolds number flows can be better modelled by values below 1200. The parameter α in the outer region formula is obtained from

$$\alpha = \frac{0.0168}{F^{2.5}} = 0.0168 \Big/ \left[1-\beta\frac{\partial u/\partial x}{\partial u/\partial y}\right]^{2.5}$$

where the nondimensional factor F denotes the ratio of total turbulence energy production to the shear-stress-related turbulence energy production, evaluated at the location of maximum shear stress

$$F = 1 - \left[\frac{(\overline{u'^2} - \overline{v'^2})\,\partial u/\partial x}{-\overline{u'v'}\,\partial u/\partial y} \right]_{(-\overline{u'v'})_{max}}$$

The ratio of the time-averaged quantities above can be approximated by a function of $R_T = \tau_w/(-\overline{u'v'})_{max}$

$$\beta = \left[\frac{\overline{u'^2} - \overline{v'^2}}{-\overline{u'v'}} \right]_{(-\overline{u'v'})_{max}} = \begin{cases} \dfrac{6}{1+2R_T(2-R_T)} & \text{for } R_T < 1 \\ \dfrac{1+R_T}{R_T} & \text{for } R_T \geq 1 \end{cases}$$

Since this turbulence model is not validated for separated flow, eddy viscosities in regions of backflow correspond to those of the adjacent upstream station at the same η-coordinate.

Transition, if not available from other sources, currently is predicted by an empirical data correlation expressed in terms of the Reynolds numbers based on momentum thickness and streamwise coordinate at onset of transition

$$R_{\theta_{tr}} = 1.174\left(1 + \frac{22400}{R_{x_{tr}}}\right) R_{x_{tr}}^{0.46}$$

Should laminar transition occur upstream of the computed point of transition, then transition is redefined at the point of laminar separation.

4. SAMPLE CALCULATIONS

This chapter will focus on sample calculations reporting on the influence of turbulence model and loci of transition, as well as on the sensitivity of calculations to the choice of the relaxation parameter. Further calculations, referring to the variation of air inlet angle and Reynolds number, are intended to demonstrate the code's abilities to predict the phenomena of low Reynolds number and high angle of attack flow regimes. No comparisons with experimental data will be presented in this report. However, the severe deviation of early calculations from experimental results, together with numerical breakdowns and convergence problems, revealed the need for a modification of the turbulence model in the low Reynolds number regime. Accordingly, the transition length has been reduced, resulting in fewer numerical troubles and improved agreement of computational and experimental results. Since the development of the code is not completed yet and further improvements are to be expected, the final evaluation, including the presentation of comparisons with experiments, is still to come. All the results describe flows past cascades, whose blades are staggered by an angle of 45 degrees and whose solidity amounts to 0.78. Cross sections of the NACA-65 series compressor blade family were selected in consideration of available experimental data. In the following, results of test case computations and a brief analysis of them will be given.

Figures 5, 6, 7, and 8 show the convergence histories as a function of the relaxation parameter ω, which has a major influence on the number of iterations required to obtain converged results. Relaxation is meant to ensure or to accelerate convergence. The lift coefficient based on inlet velocity is taken as convergence indicator, although other choices are equally possible. Figure 5 presents the convergence behaviour of a high Reynolds number flow at zero incidence. The geometrical input consists of 51 blade coordinates, taken from the original NACA publication. The code works with recomputed coordinates, which are cosine-distributed along the chord length. Subplot (a) refers to 51 of these recomputed coordinates, subplot (b) to 97. The upper plot of figure 5 displays a desirable convergence behaviour, wherein all curves approach the same lift coefficient after a finite number of iteration cycles. Maximum acceleration is achieved by a relaxation parameter of 2.0 or slightly higher. Smaller relaxation parameters delay convergence, higher relaxation parameters can lead to numerical breakdowns. The lower plot of figure 5 indicates a numerical instability, which seems to be related to the panel code. There is no evidence that these oscillations are due to unsteady loci of transition. The oscillations of the lift coefficients are stable in amplitude and the mean of all oscillations tends towards a single value. Since the amplitude of the oscillations amounts only to half

a percent of the lift coefficient, results might even be regarded as converged. Probably not the panel code itself, but the procedure how coordinates are recomputed is responsible for the instabilities. The currently used interpolation functions are - unlike spline functions - continuous in values of functions only, not in derivatives. If the number of recomputed coordinates strongly exceeds the number of input coordinates, then the used interpolation algorithm might give rise to irregular shapes in the leading and trailing edge areas, where points are packed because of the cosine-redistribution.

The same cascade configuration at the same incidence, but at a much smaller Reynolds number leads to numerical divergence and numerical termination of the calculation, as can be seen from figure 6. Subplots (a) and (b) refer again to 51 and 97 recomputed coordinates. Calculations have been performed up to 40 iteration cycles, of which only the first 20 are shown. Some of the computations break down between cycle 20 and 40, the remaining computations keep changing, but do not get terminated within 40 cycles. Furthermore, computations for different relaxation parameters do not approach a common lift coefficient. Numerical breakdowns are either due to a failure of the Newton iterations at a particular streamwise position to converge, or due to negative external velocities as an artificial result of extensively separated boundary layers. These difficulties are related to unrealistically large regions of flow separation, which are caused by the turbulence model. The original CS-model, being based on high Reynolds number data, overestimates the length of transitional flow for low Reynolds numbers, which in conjunction with bubble transition can trigger dramatic deviations from realistic flow results.

Transitional flow in the CS-model is accounted for by an intermittency factor γ_{tr}

$$\gamma_{tr} = 1 - \exp\left[-\frac{u_e^3}{G_{\gamma_{tr}} \nu^2} R_{x_{tr}}^{-1.34} (x - x_{tr}) \int_{x_{tr}}^{x} \frac{d\xi}{u_e} \right]$$

This factor, being a transient function with values 0 at onset of transition and 1 at fully turbulent flow, avoids an abrupt transition from laminar to turbulent flow by smoothing out the step-shaped change from kinematic to eddy viscosity. The length of transitional flow is mainly determined by the empirical constant $G_{\gamma_{tr}}$, which was set 1200 in the original CS-model. This choice makes the transitional region of low Reynolds number flows spreading too far into the turbulent region. Consequently, low Reynolds number flows with a $G_{\gamma_{tr}}$ of 1200 are more likely to separate and less likely to reattach in the transitional region. Numerical experiments (see also figures 9 to 15) imply that low Reynolds number flows require smaller constants $G_{\gamma_{tr}}$. Figure 7 shows the results of the same low Reynolds number flows as in figure 6, using a slightly modified turbulenec model, but still computing the point of transition. Subplot (a) corresponds to a $G_{\gamma_{tr}}$ of 120, subplot (b) to a $G_{\gamma_{tr}}$ of 12, respectively. Calculations seem to converge now, however at retarded rates of convergence when compared with the high Reynolds number case. Most of the computations end up with oscillations of the lift coefficient, which originate here from moving transition points. Fixing transition on both upper and lower surface turns the oscillating lift histories of figure 7 into smooth curves, which are given in figure 8. Transition on the uppper surface is assumed at midchord, transition on the lower at 70 percent of chord. Fixing transition supresses a degree of freedom, because of which only carefully selected locations might work out. The above chosen loci reflect the most upstream positions, where transition ever has been experienced within 20 cycles. Recapitulating, reasonable results for a low Reynolds number flow could be accomplished in the investigated case by the following provisions:

1. The extension of transitional flow has to be narrowed by decreasing an empirical constant in the CS-model.
2. The loci of transition have to be fixed at reasonable locations.

The following 6 plots offer some insight into the convergence histories of the low Reynolds number flows, whose lift histories are given in figure 6.a and 8.a, respectively. Figures 9, 11, and 13 refer to the unsuccessful calculation, using the original CS-model, computed transition, and a relaxation parameter of 2. Figures 10, 12, and 14 display the results of an equivalent calculation, but now using the modified turbulence model with a $G_{\gamma_{tr}}$ of 120, fixed transition at midchord on the upper and 70 percent of chord on the lower surface, and a relaxation parameter of 2. The histories of pressure coefficient, local skin friction coefficient, and displacement thickness are presented for the first 10 cycles. Figure 9 and 10 give the histories of pressure distributions, showing the developments from purely inviscid results (indicated by iteration number 0) to those altered increasingly by viscous displacement effects. Pressure distributions are rather insensitive compared to the

more dramatic changes of the lift coefficients during the iteration process. With the exception of the trailing edge, pressure distributions keep looking the same, only flow separation leaves some marks - a sort of flat - on the pressure distributions. The longer flats in figure 9 suggest a more extended flow separation than in figure 10.

Figures 11 and 12, which show the developments of local skin friction distributions, prove this assertion. Two flow phenomena can be read from skin friction distributions: Flow separation occurs at the point of zero skin friction and transition is accompanied by a steep increase in skin friction. A closeup of the numerically unstable computation of figure 11 indicates that laminar flow separation takes place a few percent upstream of midchord on the upper surface, but turbulent reattachment, which closes the bubble usually not too far downstream of the point of separation, seems to be omitted. At the streamwise position, where fully turbulent flow is established, backflow dominates so that the boundary layer is not able to return to the wall. The lower surface exhibits laminar separation too, but there the flow does form a bubble. These results are considered unsatisfactory, because one would not expect a severe trailing edge separation, extending over half the chordlength, in cascades with only slightly cambered blade sections at zero incidence, even when exposed to low Reynolds numbers. The results of figure 12, which were obtained by using the modified turbulence model and fixed transition, fit much better both our expectations and experiments. Forced transition makes the results in some way less realistic, but forced transition is necessary to avoid oscillations. Transition is followed on both surfaces by a steep increase in skin friction, being caused by the fuller velocity profiles of turbulent boundary layers. The locations of transition, which had been chosen specifically to circumvent numerical instabilities, seem to suppress laminar separation and bubble transition. The flow remains completely attached on the lower surface, while it separates on the upper surface close to the trailing edge. This turbulent trailing edge separation can be noticed for the first time in cycle 3, and a few cycles afterwards a steady separation over 6 percent of chordlength has been established.

Displacement thickness measures the deviation of viscous flow from inviscid flow, i.e. it tells how far streamlines are shifted from the surface by viscous effects. Uneven displacement on upper and lower surface causes a lift loss compared to the inviscid flow case. Figure 13 and 14, which present the developments of displacement thickness distributions, depict the differences of displacement thickness on the upper and lower surface, which tend to uncamber the airfoil. Displacement thickness at the trailing edge - like the lift coefficient - proves to be an excellent convergence indicator. The breakdown of calculations in figure 13 is preceded by an impressive growth of displacement thickness at the trailing edge on the upper surface. Constant values since cycle 8 signal convergence of that case shown in figure 14. Both figures have marks, left by transition and separation. Transition is usually accompanied by slight drawback in the steady growth of displacement thickness, which can be seen clearly on both surfaces. Separation dramatically increases the growth of the displacement thickness, which is well demonstrated at the trailing edge on both upper surfaces.

Figure 15 compares the results for two different airfoil sections of the NACA 65-series compressor blade family, both of which are arranged in a staggered cascade of relatively low solidity. The variations of lift coefficient based on inlet velocity and turning angle as a function of air inlet angle are given for both inviscid and converged viscous flow computations. The blade sections are the 10 percent thick NACA 65-410 and NACA 65-(12)10, whose camber is indicated by the first number after the dash, denoting the design lift coefficient in tenths for the isolated airfoil. The high Reynolds number did allow calculations to be carried out with the original CS-turbulence model and having the points of transition computed. In spite of the high Reynolds number inviscid and viscous results are clearly different due to viscous displacement effects, which are more pronounced in case of the more cambered blade section. The beginning breakaway of the viscous curves from their inviscid counterparts, observed in the left subplot, suggests onset of stall at an air inlet angle of 62 degrees for the investigated cascade. Calculations for air inlet angles at and beyond stall could not be performed successfully. Therefore the plots were terminated before approaching angles of deep stall.

The following three plots reveal the dependence of local flow quantities on air inlet angle for that cascade flow, whose lift variations are given in the left plot of figure 15. The variations of pressure, skin friction, and displacement thickness - all in dimensionless form - are shown in figure 16, 17 and 18. The distributions of pressure coefficients, based on the dynamic pressure of inlet velocity, provide information about the blade loadings. Pressure peaks result from highly accelerated flow around the leading edge, when the stagnation

point is relatively far away from the geometric leading edge. Only those pressure distributions, which correspond to air inlet angles around the design lift coefficient, can avoid velocity-peaks at the leading edge. The flattening of pressure distributions in the trailing edge area indicates separation on the upper surface for the highest incidence angles. None of the flows exhibits a laminar separation on either upper or lower surface, which anyway would not be expected for such a high Reynolds number. At air inlet angles of 60 and 62 degrees turbulent trailing edge separation (without reattachment) does occur, extending over 4 and 20 percent of chordlength, respectively. Transition from laminar to turbulent flow regime is accompanied by a step-shaped increase of skin friction, which permits the identification of transition in the skin friction plots. With increasing incidence transition is shifted on the upper surface towards the leading edge, while the lower surface experiences a reverse move of transition. The development of displacement thickness distributions gives a good indication how much flow is disturbed by viscous effects. Generally, the perturbation increases with higher incidence. However, for positive incidence the lower surface shows no significant changes in the distributions of displacement thickness. It is the difference between the displacement thickness on upper and lower surface, that entails the loss of lift. Since the difference is more pronounced at high incidence, those flows depart more strongly from the inviscid ideal.

Finally, the last four plots are intendend to promote the basic understanding of viscous flows past cascades. Velocity profiles along pressure and suction surface are shown for four representative flow regimes. The vertical scales of the velocity profiles had been enlarged to achieve a good resolution. allowing the illustration of marginal backflow. Figure 19 and 20 investigate the effect of the Reynolds number on viscous flow results. Flows at Reynolds numbers of 6 million and 245,000 were chosen to represent the high and low Reynolds number regimes at an air inlet angle, which corresponds roughly to the design lift coefficient. Both cases had been examined and depicted in terms of other flow quantities on previous occasions in this report: The lift histories of the high Reynolds number flow in figure 5.a, the lift histories and the developments of pressure. skin friction. and displacement thickness for the low Reynolds number flow in figures 8.a. 10. 12. and 14. The more obvious effects as the Reynolds number decreases are a more pronounced growth of boundary layers and a shift of transition points towards the trailing edge. The locations of transition in figure 20 have been specified (to avoid numerical instabilities); however, they do reflect the most upstream positions, where transition ever occured in the computation. The absence of a somehow expected transition bubble in figure 20 is due to that forced transition. which. if prescribed upstream of the laminar separation point. can eliminate the bubble entirely or reduce its extent. Furthermore. these figures demonstrate the different shapes of laminar. turbulent. and separating velocity profiles. The rapid flow acceleration immediately at the surface. as is typical for turbulent profiles. contrasts the gradual flow acceleration of laminar profiles.

The influence of the air inlet angle on boundary layer results is investigated in figure 21 and 22. Air inlet angles of 48 and 58 degrees have been selected to show flow regimes of cascades at negative and positive incidence. As the air inlet angle increases. velocity profiles on upper and lower surface differ more and more. resulting in strongly asymmetric displacement on the upper and lower surface. Transition on upper surface moves with increasing air inlet angle towards the leading edge. while on the lower surface the laminar flow region spreads with increasing air inlet angle. eventually leading to completely laminar flow. as can be seen from figure 22. Low Reynolds numbers and small or negative incidence angles can give rise to bubble transition. which is illustrated in figure 21. Flow on upper surface remains laminar until midchord. separates then. becomes transitional. and reattaches as a turbulent boundary layer. Strongly decelerating flows can even cause the separation of turbulent boundary layers. The increasing region of backflow on the upper surface at the trailing edge is responsible for the loss of lift. as the angle of attack approaches stall. All four velocity profile plots give a good indication. how boundary layers grow. how they develop regions of reversed flow. and also how the external velocity changes over the blade.

5. CONCLUSIONS

This report presents a numerical method to analyse viscous incompressible flows past 2-d cascades. Cebeci and collaborators developed a viscous-inviscid interaction method, which accomplishes a complete flow solution by treating alternately inviscid and viscous flow regimes. Inviscid flow equations are solved by means of a standard panel method, viscous flow equations are approximated by boundary layer equations, whose solution is determined by a finite difference scheme. The essence of the method is an interactive boundary condition, which forces viscous and inviscid flow to merge smoothly at the boundary layer edge. It is the numerical implementation of this condition, which, by prescribing a linear combination of external velocity and displacement thickness, avoids the difficulties incurred when either direct or inverse boundary layer methods are employed. The current method is—like Navier-Stokes-solvers—capable of computing viscous flows including flow separation, but in contrast to Navier-Stokes-solvers, at significantly lower computing costs.

The potential and capabilities of the method have been demonstrated for flows past cascades of moderately cambered blade sections over a range of Reynolds numbers and air inlet angles. The investigated flows involved both laminar separation bubbles and turbulent separation without reattachment. The procedure seems to work reliably for high Reynolds numbers and small incidence angle, but encounters difficulties in cases of low Reynolds numbers and highly loaded blades. Numerical experiments indicated the need for a modified turbulence model in low Reynolds number flows, in which the original model overestimated the length of transition. The location of transition evidently has a considerable influence on computed boundary layer results. Numerical instabilities had to be overcome partly by specifying transition, which might cause a deviation from the true flow behaviour because of surpressed laminar separation bubbles. Since the method is not yet capable of handling highly cambered blade sections or incidence angles corresponding to stall and post-stall, further improvements are necessary to obtain a more universal code. Future work should attempt a more accurate modelling of both separating and transitional flow regimes. In the near future progress may be made by

1. Including the effects of viscous wakes, which should improve our ability to predict separated flow.
2. Relaxing the FLARE-approximation by introducing an upwind differencing scheme for streamwise derivatives.
3. Reconsidering some of the numerical features, like interpolation and smoothing algorithms.

Ultimately, a satisfactory analysis of viscous cascade flows will require

4. A better understanding of the physics of transition, eventually leading to a more reliable prediction of transition.
5. A more advanced interaction model to resolve the difficulties at high incidence angles.

ACKNOWLEDGMENTS

This research was sponsored by the Naval Air Systems Command under Contract N-62271-85-M-0437. The author wishes to express his appreciation to Prof. Platzer for his support and many helpful discussions. Prof. Cebeci's help and the access to his codes are gratefully acknowledged.

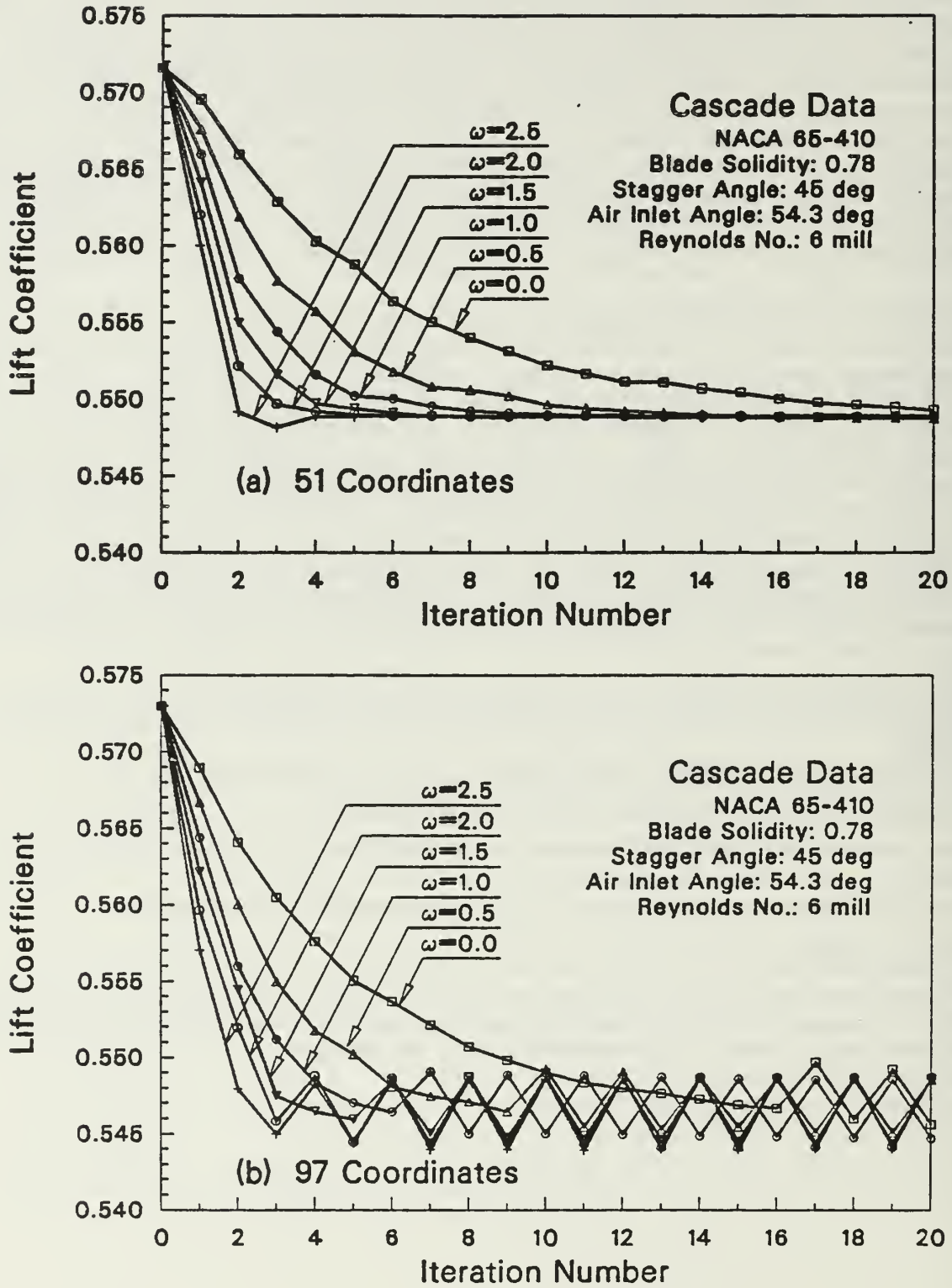

Fig. 5. Lift histories of a converging case. Flow past a staggered cascade at high Reynolds number

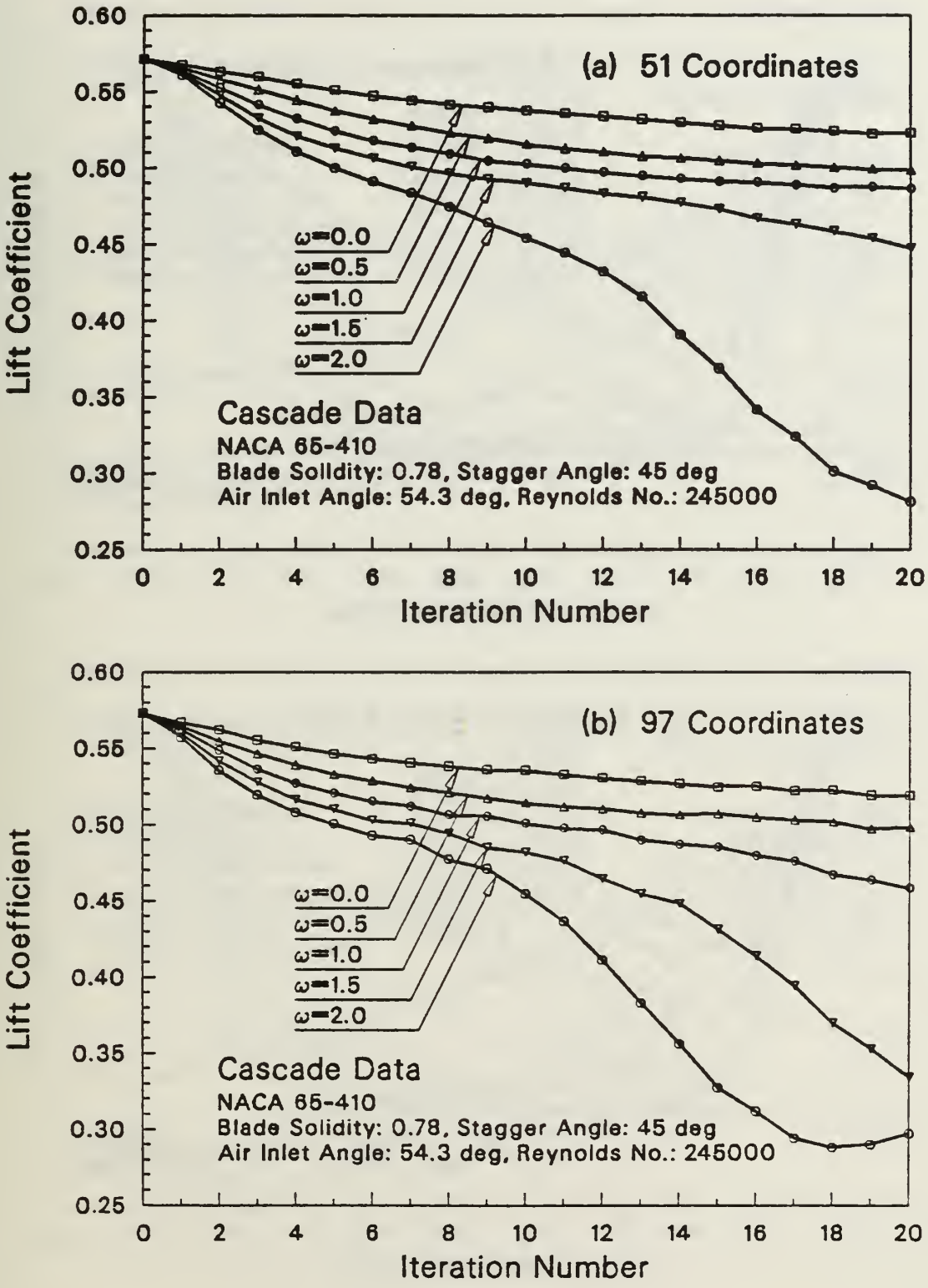

Fig. 6. Lift histories of a diverging case. Flow past a staggered cascade at low Reynolds number

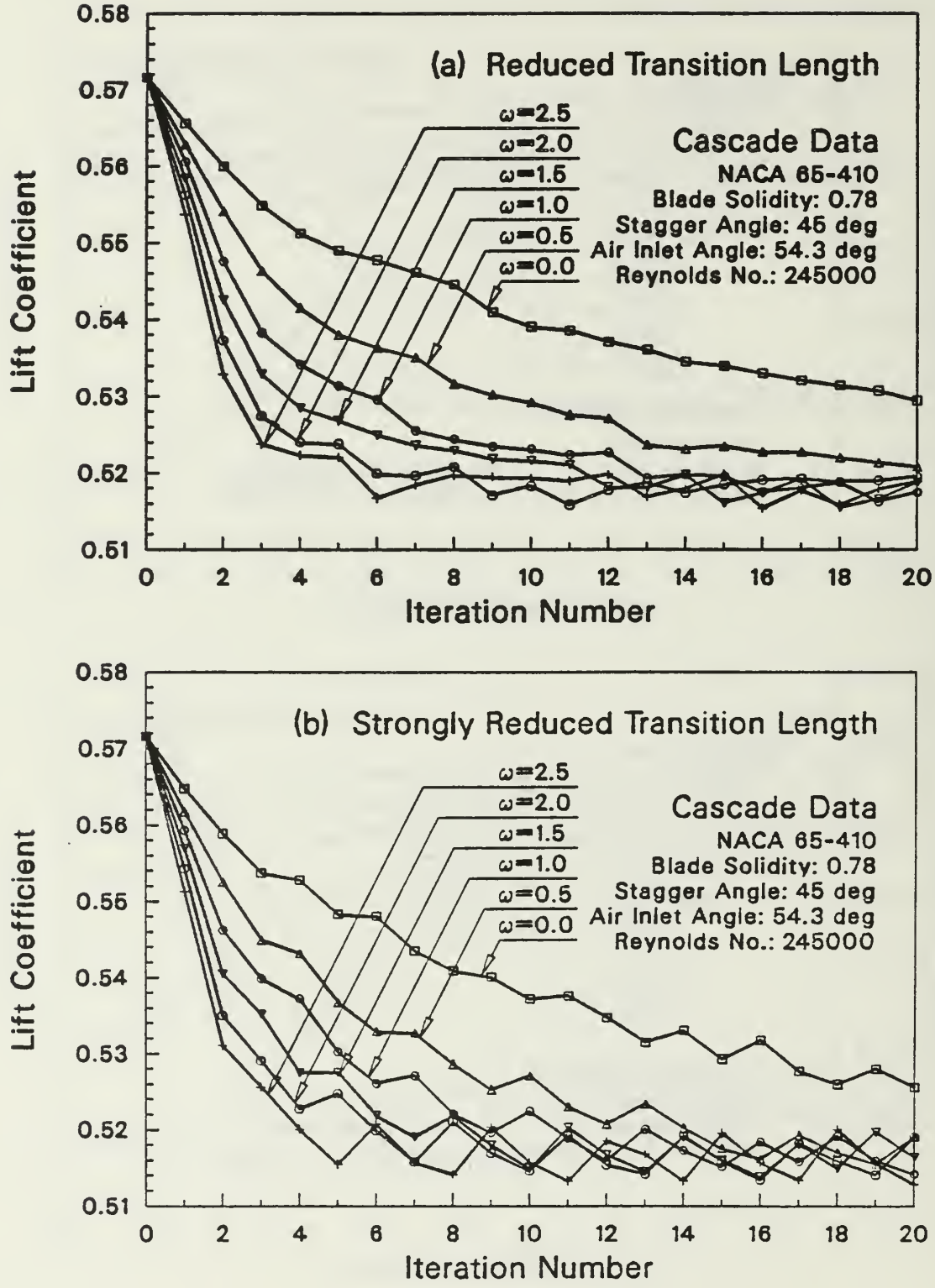

Fig. 7. Lift histories of a slightly oscillating case. Flow past a staggered cascade at low Reynolds number with a changed turbulence model

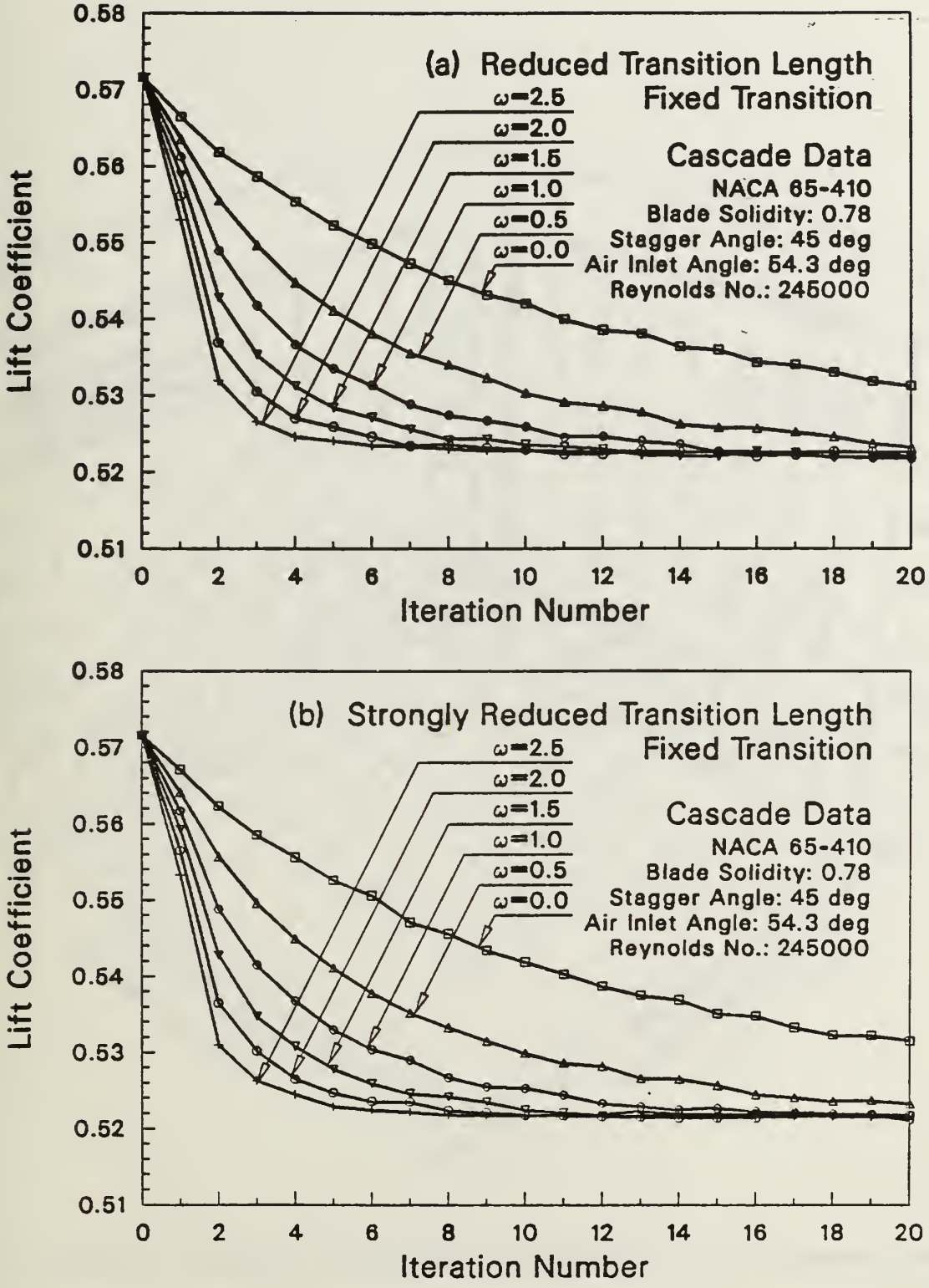

Fig. 8. Lift histories of a converging case. Flow past a staggered cascade at low Reynolds number with a changed turbulence model and fixed transition

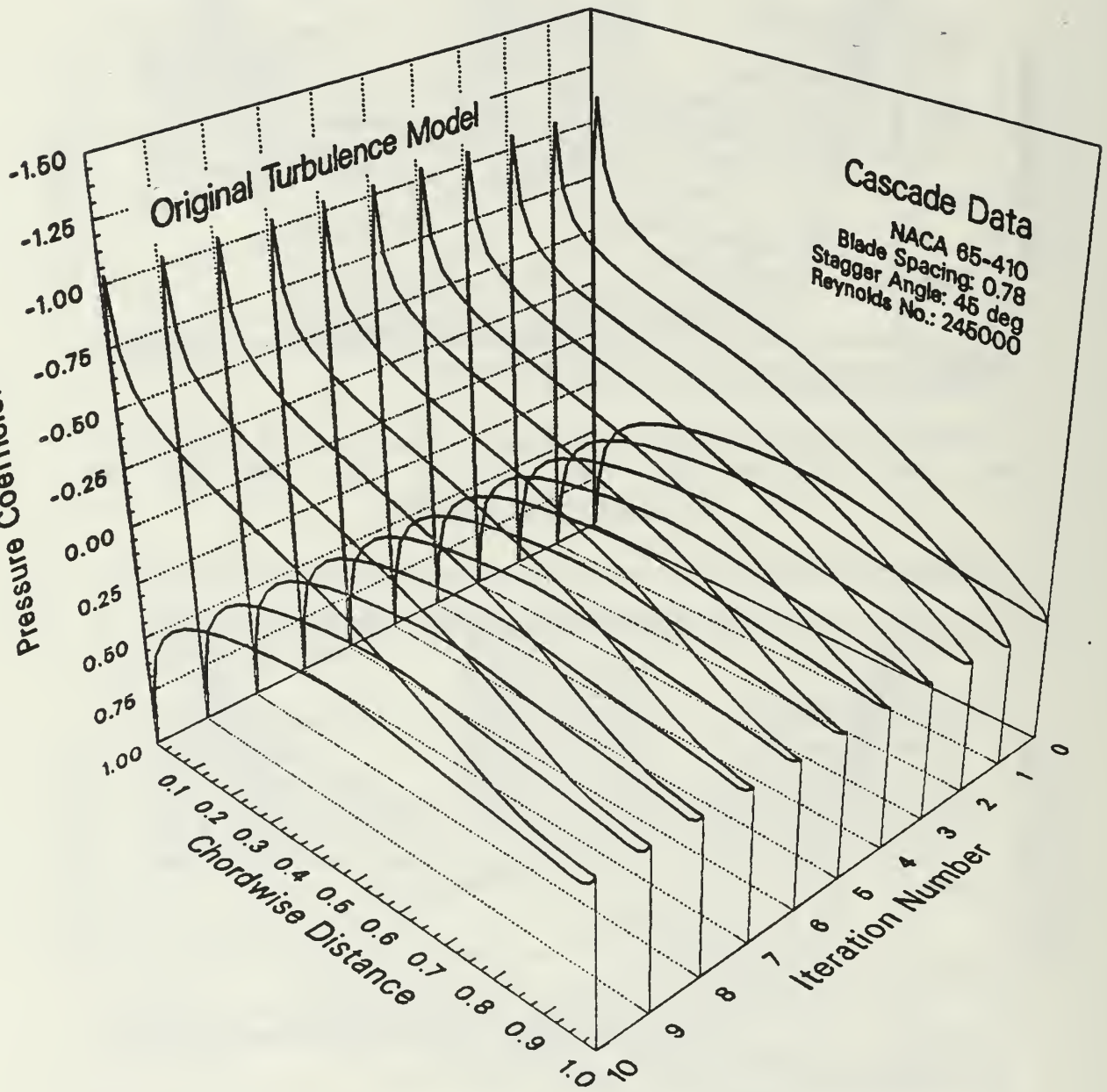

Fig. 9. Development of pressure distributions with number of iterations for a diverging case

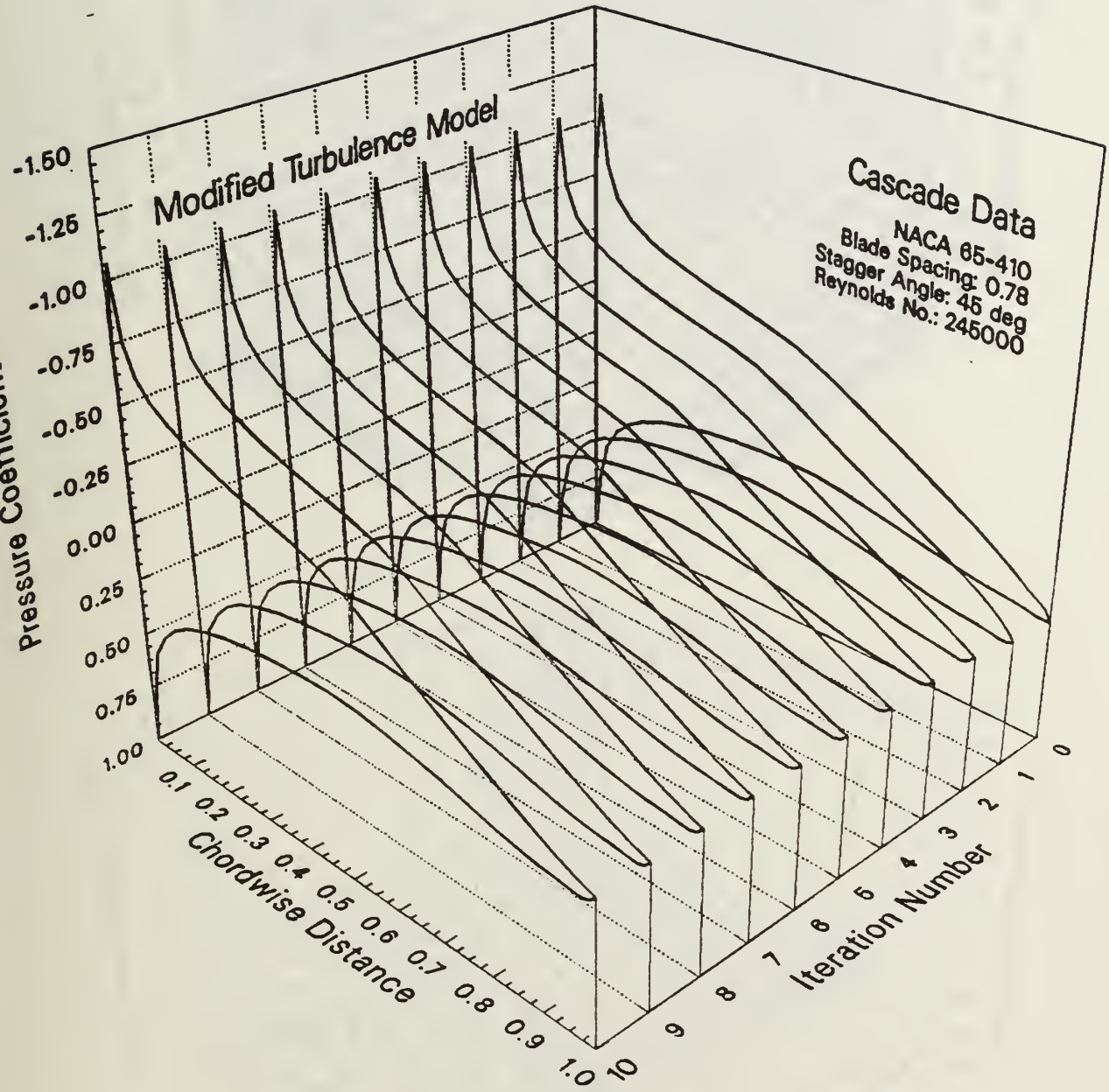

Fig. 10. Development of pressure distributions with number of iterations for a converging case

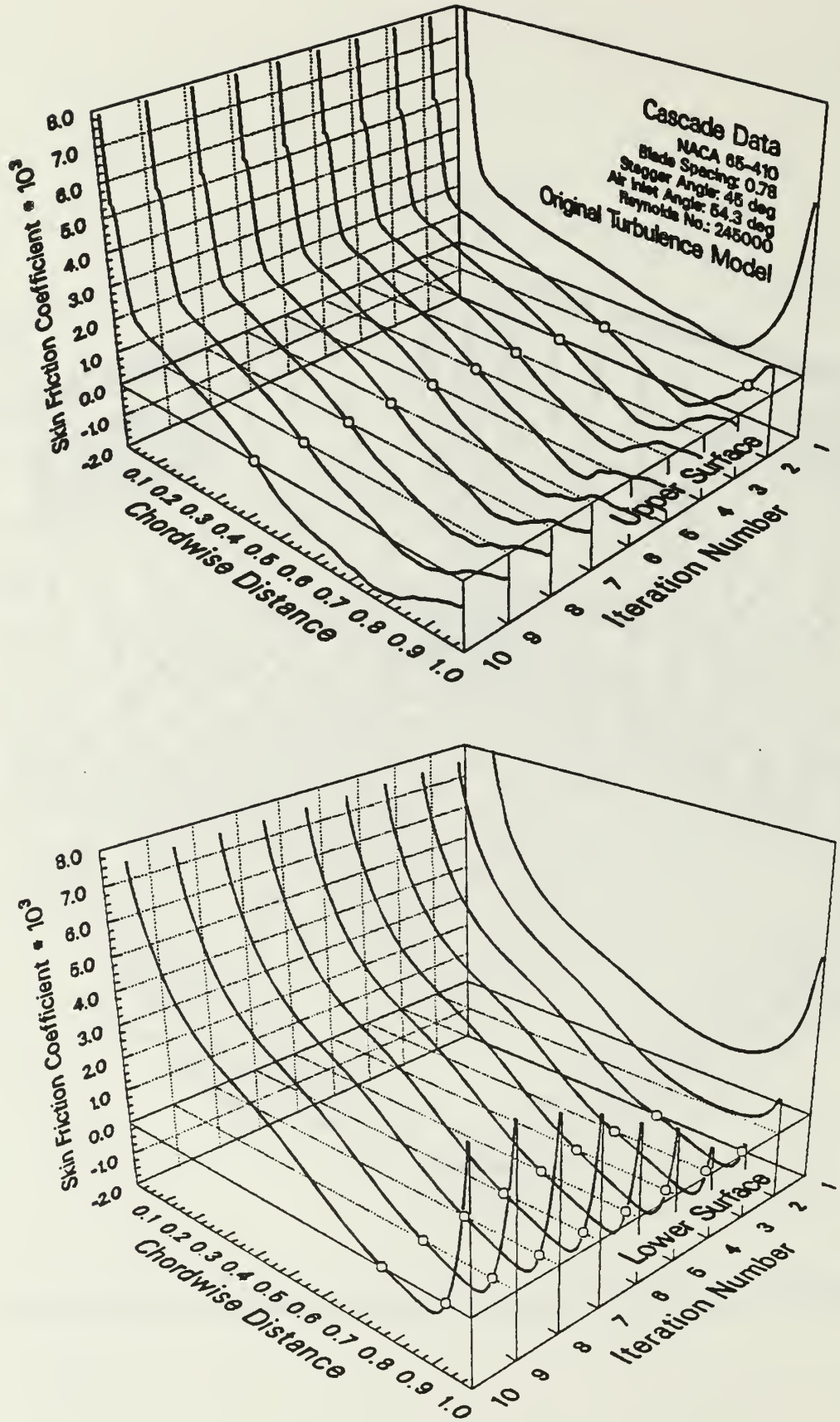

Fig. 11. Development of local skin friction distribution with number of iterations for a converging case

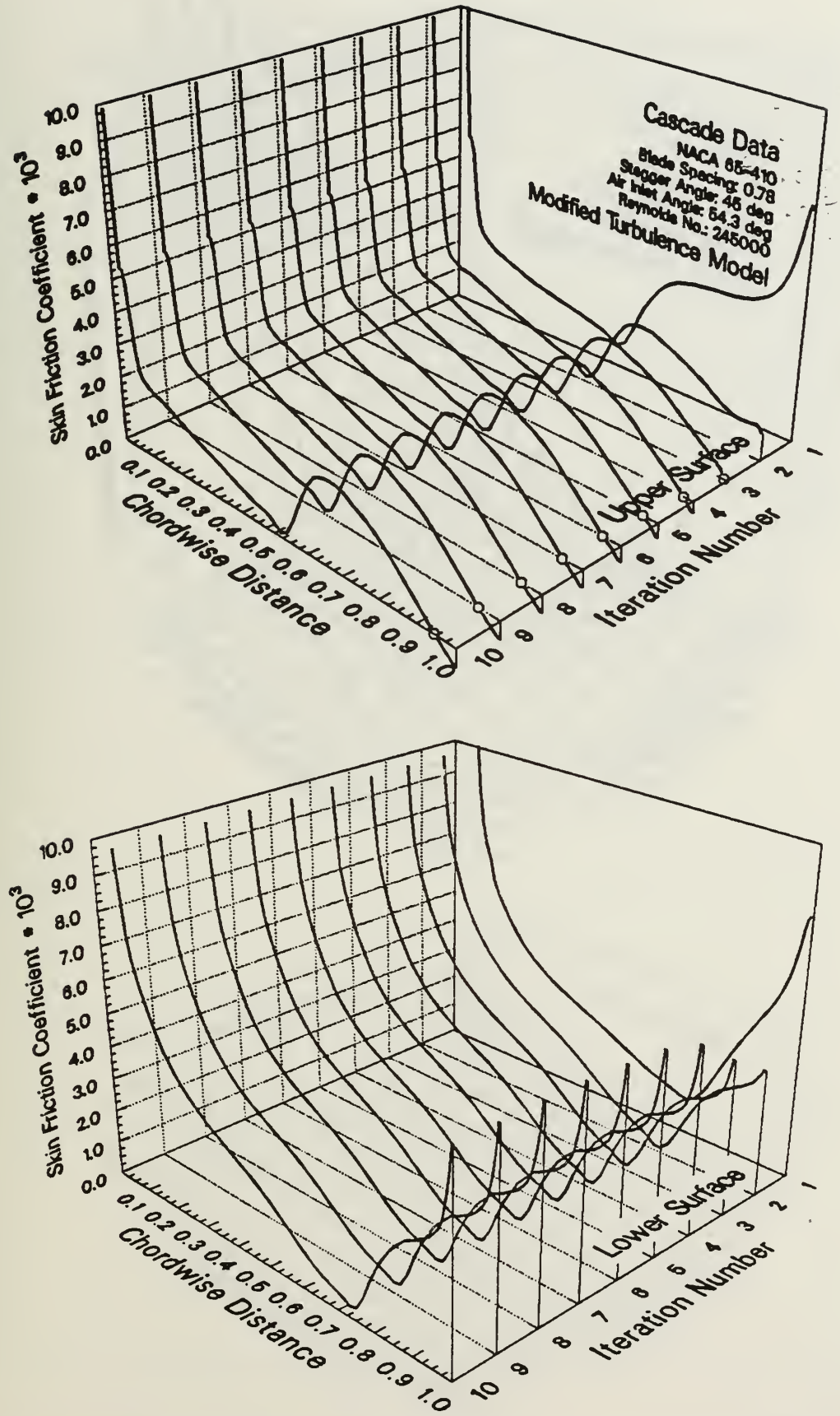

Fig. 12. Development of local skin friction distribution with number of iterations for a converging case

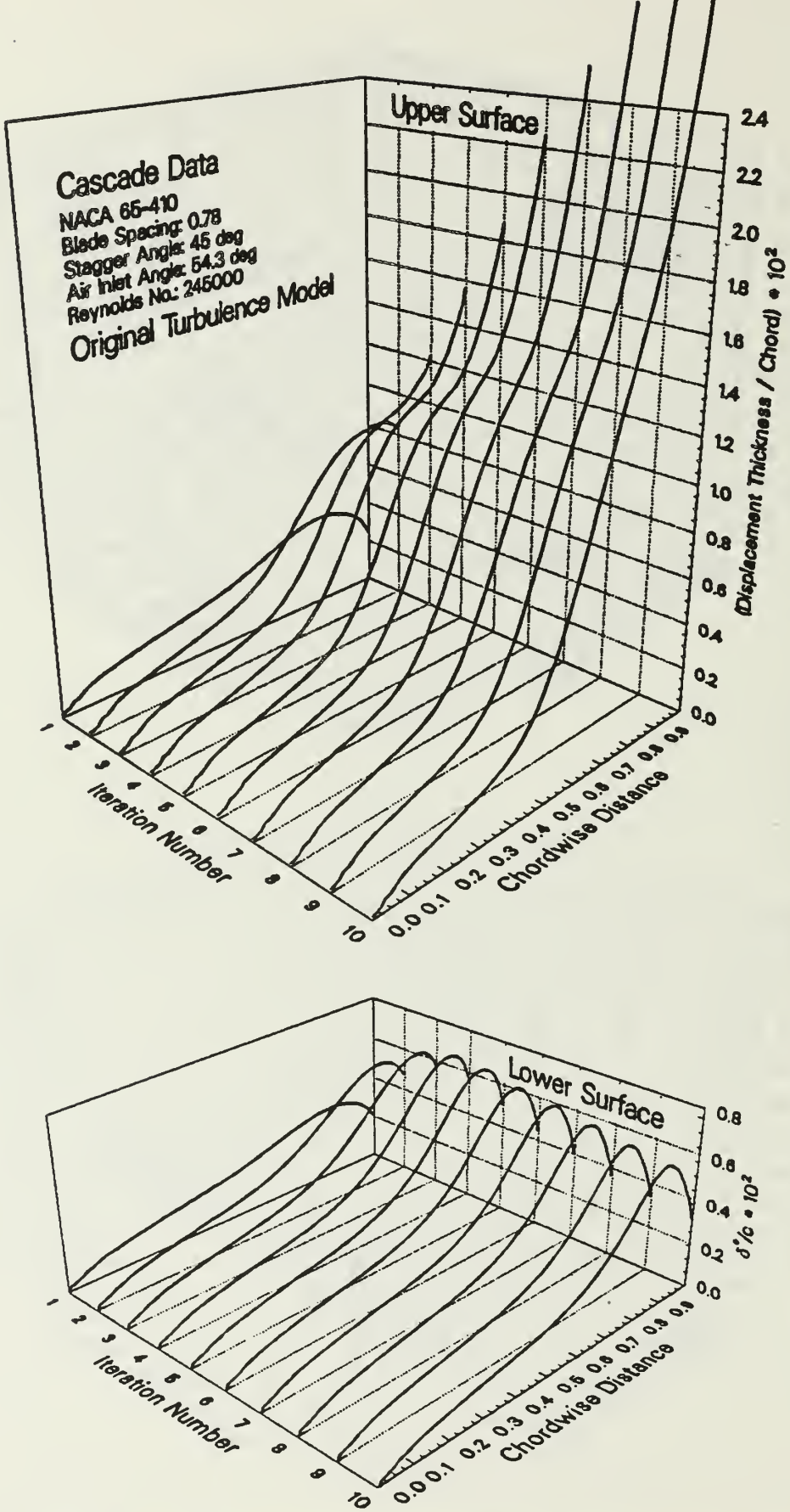

Fig. 13. Development of displacement thickness distribution with number of iterations for a diverging case

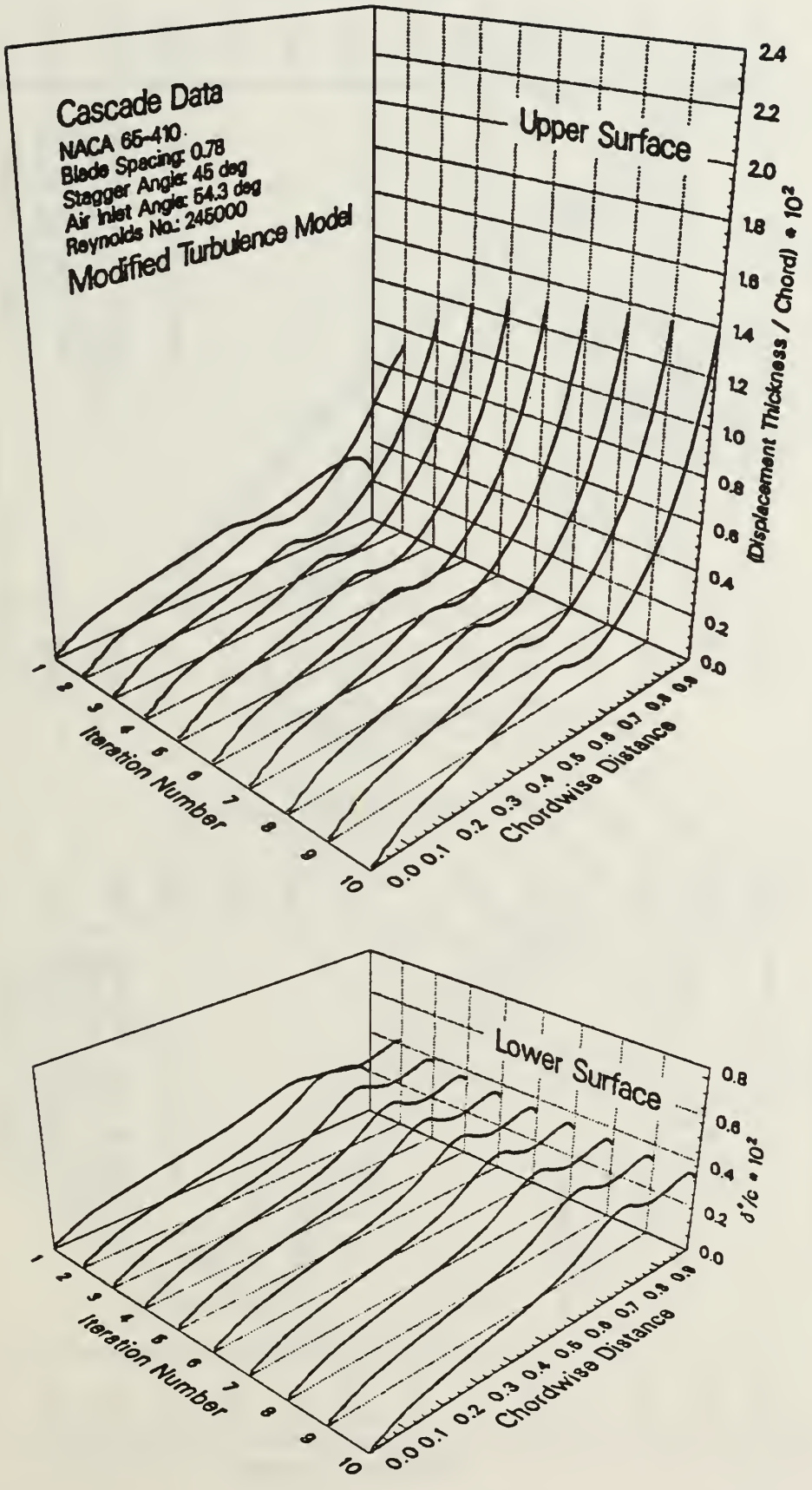

Fig. 14. Development of displacement thickness distribution with number of iterations for a converging case

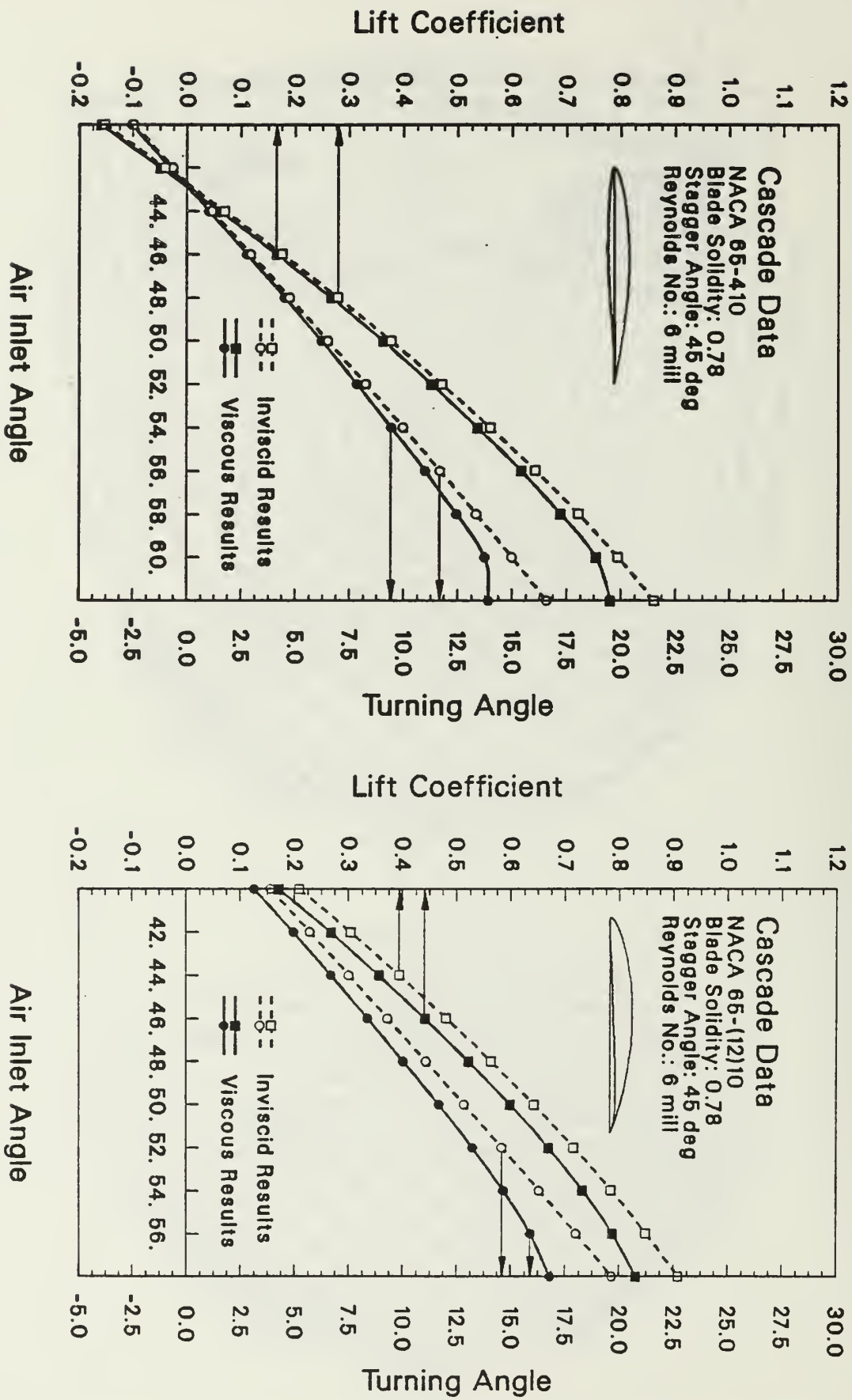

Fig. 15. Lift and turning angle as a function of air inlet angle for two different airfoil sections in cascade

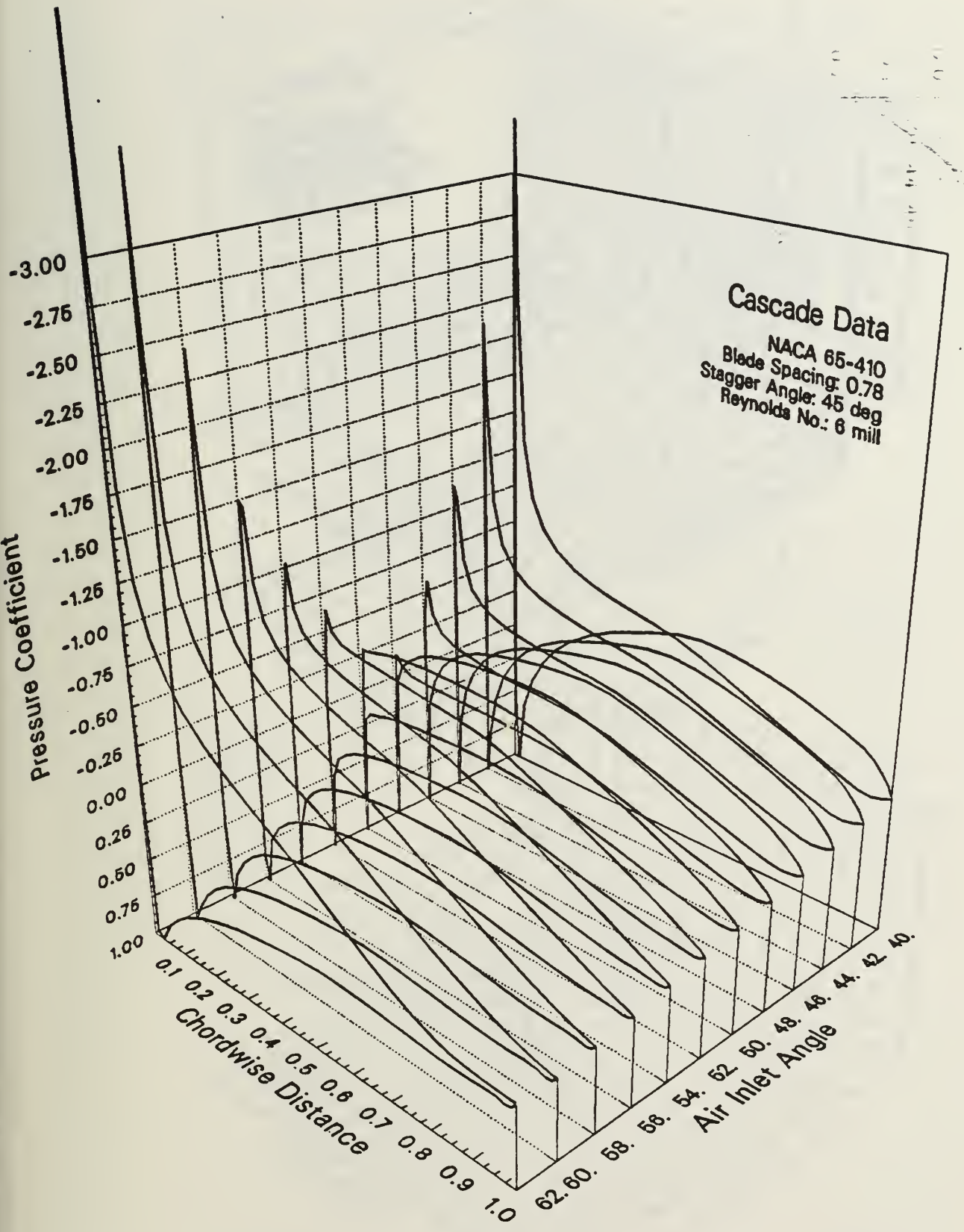

Fig. 16. Variation of pressure distribution with air inlet angle for a staggered cascade at high Reynolds number

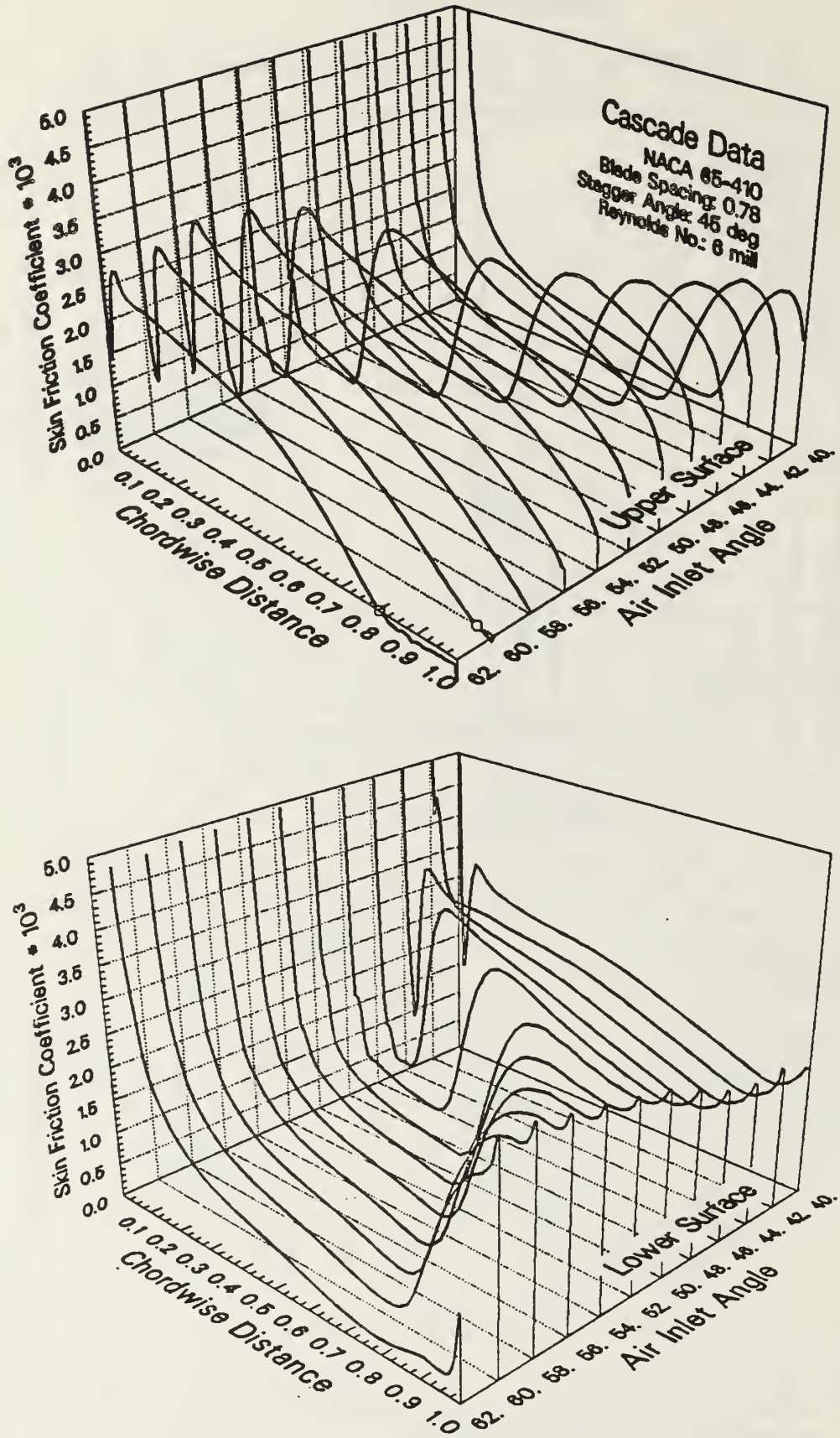

Fig. 17. Variation of local skin friction distribution with air inlet angle for a staggered cascade at high Reynolds number

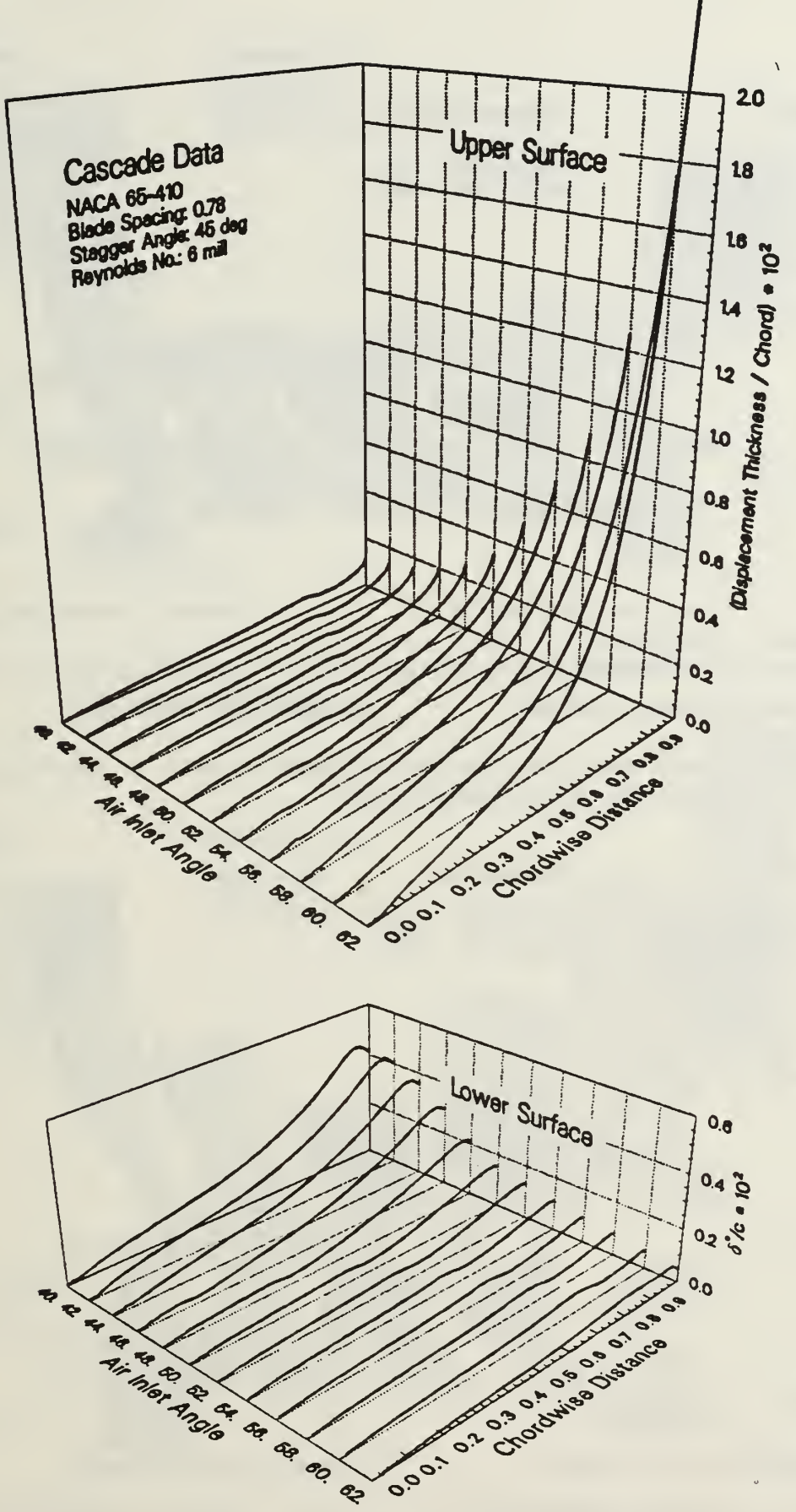

Fig. 18. Variation of displacement thickness distribution with air inlet angle for a staggered cascade at high Reynolds number

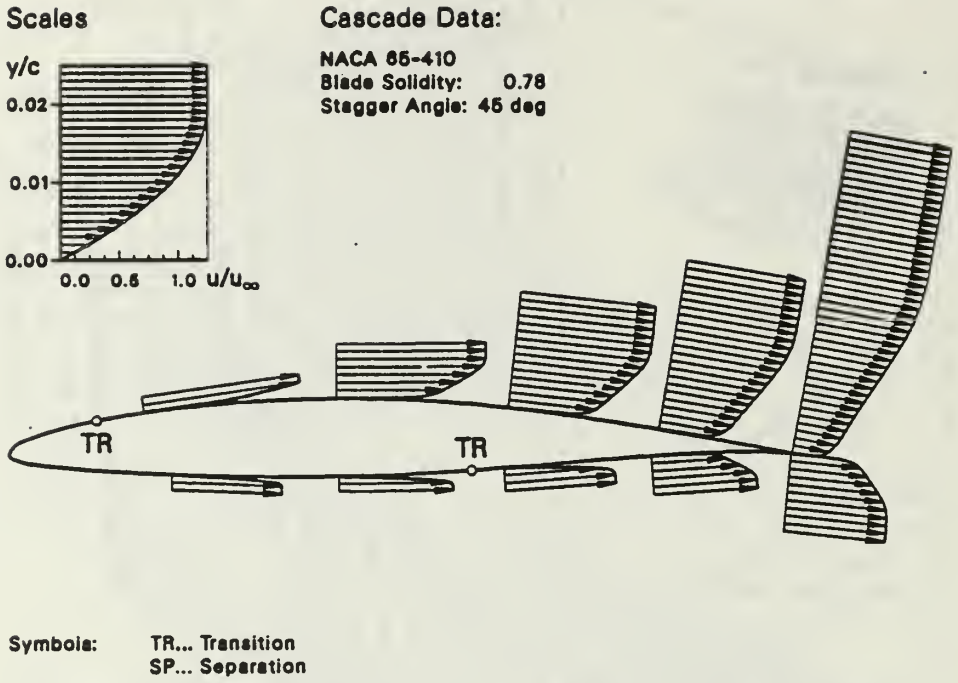

Fig. 19. Velocity profiles on a NACA 65-410 airfoil in cascade at high Reynolds number and moderate angle of attack

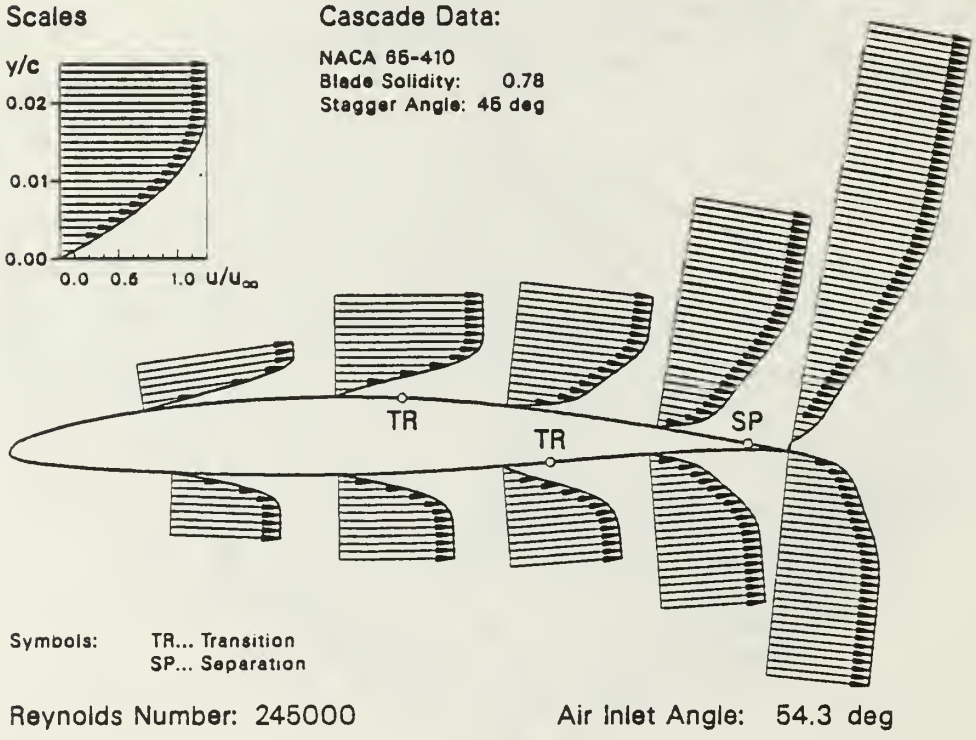

Fig. 20. Velocity profiles on a NACA 65-410 airfoil in cascade at low Reynolds number and moderate angle of attack

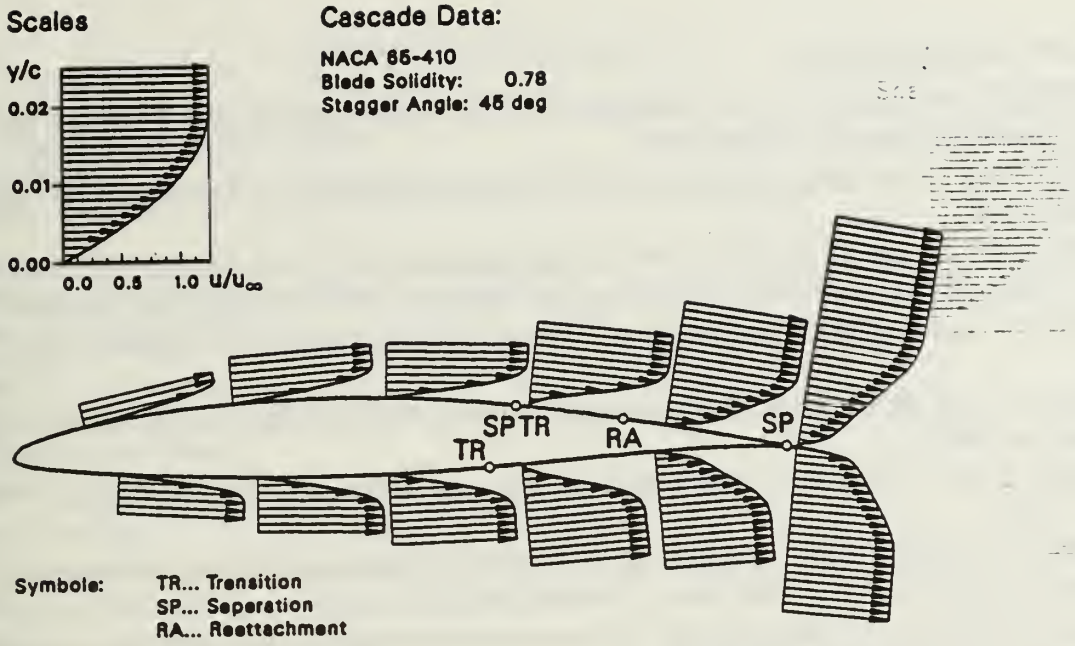

Fig. 21. Velocity profiles on a NACA 65-410 airfoil in cascade at low Reynolds number and low angle of attack

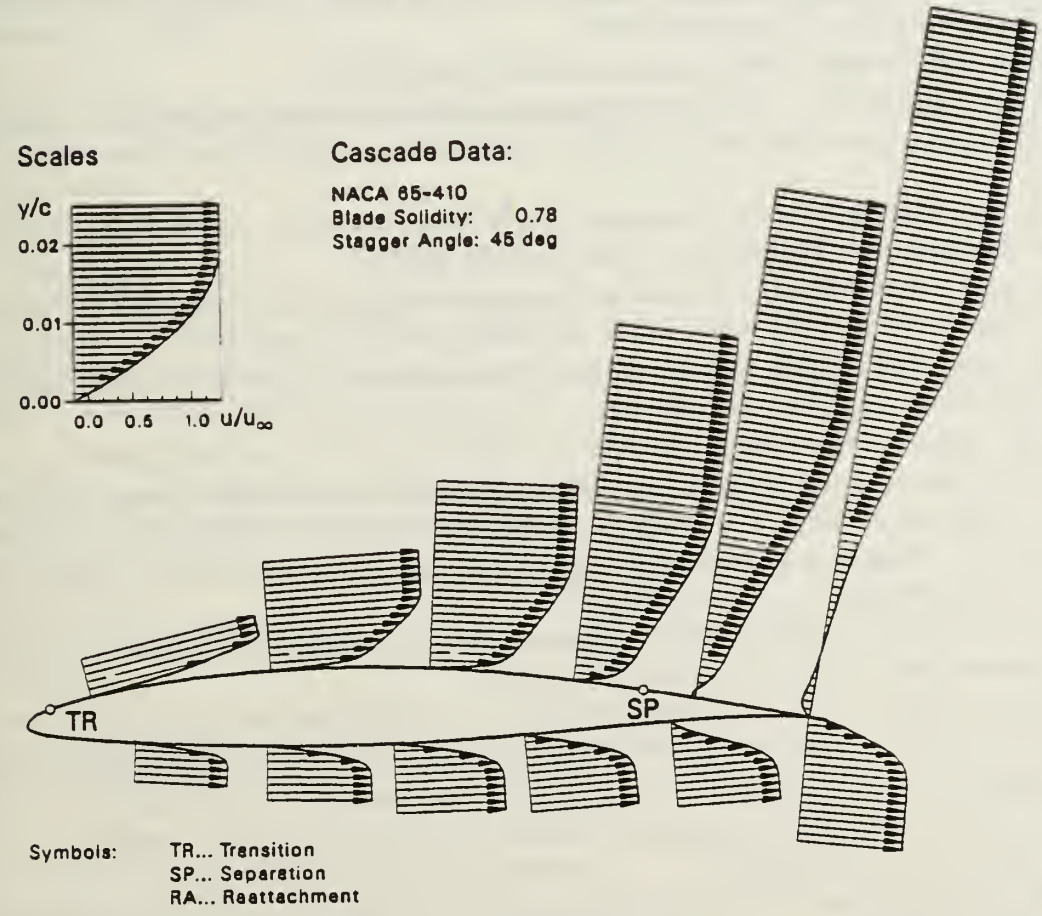

Fig. 22. Velocity profiles on a NACA 65-410 airfoil in cascade at low Reynolds number and high angle of attack

6. LIST OF REFERENCES

1. BRADSHAW, P., CEBECI, T., and WHITELAW, J.H. Engineering Calculation Methods for Turbulent Flows. Academic Press, New York, 1981.
2. CARTER, J.E. A New Boundary-Layer Inviscid Iteration Technique for Separated Flow. AIAA Paper 79-1450, 1979.
3. CATHERALL, D. and MANGLER, K.W. The Integration of the Two-Dimensional Laminar Boundary-Layer Equations Past the Point of Vanishing Skin Friction. J. Fluid Mech., Vol.26, pp.163-182, 1966.
4. CEBECI, T., and SMITH, A.M.O. Analysis of Turbulent Boundary Layers. Academic Press, New York, 1974.
5. CEBECI, T., and BRADSHAW, P. Momentum Transfer in Boundary Layers. Hemisphere-McGraw Hill, Washington, 1977.
6. CEBECI, T. (ed.) Numerical and Physical Aspects of Aerodynamic Flows II. Springer Verlag, New York, 1984.
7. CEBECI, T., CLARK, R.W., CHANG, K.C., HALSEY, N.D., and LEE, K. Airfoils with Separation and the Resulting Wakes. J. Fluid Mech., Vol.163, pp.323-347, 1986.
8. CEBECI, T., HESS, J.L., and LEE, K.H. An Interactive Procedure for Cascade Flows. NAVAIR-Report, Contract No. N00014-84-K-0740, 1986.
9. GIESING, J.P. Extension of the Douglas Neumann program to Problems of Lifting Infinite Cascades. Douglas Aircraft Company Report No. LB31653, 1964.
10. GOLDSTEIN, S. On Laminar Boundary Layer Flow near a Position of Separation. The Quart. J. Mech. & Appl. Math., Vol.1, Part 1, pp.43-69, 1948.
11. GOSTELOW, J.P. Cascade Aerodynamics. Pergamon Press, 1984.
12. HANSEN, E.C., SEROVY, G.K., and SOCKOL, P.M. Axial-Flow Compressor Turning Angle and Loss by Inviscid-Viscous Interaction Blade-to-Blade Computation. ASME J. Eng. Power, Vol.102, No.1, pp.28-34, 1980.
13. HESS, J.L., and SMITH, A.M.O. Calculation of Potential Flow about Arbitrary Bodies. Progess in Aeronautical Sciences (ed. Kuchemann), Vol.8, pp.1-138, 1964.
14. KELLER, H.B. A New Difference Scheme for Parabolic Problems. In "Numerical Solution of Partial Differential Equations" (ed. Hubbard), Vol.2, Academic Press, New York, 1971.
15. KWON, O.K. and PLETCHER, R.H. Prediction of Incompressible Separated Boundary Layers Including Viscous-Inviscid Interaction. J. Fluid Mech., Vol.101, No.4, pp.466-472, 1979.
16. LIGHTHILL, M.J. On Displacement Thickness. J. Fluid Mech., Vol.4, pp.382-392, 1958.
17. MICHEL, R. Etude de la transition sur les profiles d'aile: establissement d'un critere de determination de point de transition et calcul de la trainee de profile incompressible. ONERA Rep. 1/1578A, 1951.
18. NAKAYAMA, A. Measurement in the Boundary Layer and Wake of Two Airfoil Models. Douglas Aircraft Company Report No. MDC J2403, 1982.
19. REYHNER, T.A. and FLUGGE-LOTZ, I. Interaction of a Shock Wave with a Laminar Boundary Layer. Int. J. Nonlinear Mech., Vol.3, No.2, pp.173-199, 1968.
20. SIMPSON, R.L., CHEW, Y.T., and SHIVAPRASAD, B.G. The Structure of a Separating Turbulent Boundary Layer. Part 1. Mean flow and Reynolds stresses. J. Fluid Mech., Vol.113, pp.23-51, 1981.
21. VAN DRIEST, E.R. On Turbulent Flow near a Wall. J. Aeronaut. Sci., Vol.23, pp.1007-1011, 1956.
22. VELDMAN, A.E.P. New Quasi-simultaneous Method to Calculate Interacting Boundary Layers. AIAA Journal, Vol.19, No.1, pp.79-85, 1981.
23. WU, C.-H. A General Theory of Three-Dimensional Flow in Subsonic and Supersonic Turbomachines of Axial-, Radial-, and Mixed- Flow Types. NACA TN 2604, 1952.

INITIAL DISTRIBUTION LIST

		No. Copies
1.	Defense Technical Information Center Cameron Station Alexandria, VA 22314	2
2.	Library, Code 0142 Naval Postgraduate School Monterey, CA 93943-5100	2
3.	Prof. Dr. M. F. Platzer Department of Aeronautics, Code 67Pl Naval Postgraduate School Monterey, CA 93943-5100	20
4.	Prof. Dr. T. Cebeci Director. Center for Aerodynamic Research California State University Long Beach, CA 92840	1
5.	Dr. A. K. Amos Manager, Airbreathing Propulsion Air Force Office of Scientific Research Andrews Air force Base Washington, D.C. 20031	1
6.	Prof. Dr. A. Bölcs Laboratoire de Thermique Appliquée et de Turbomachines Ecole Polytechnique Fédéderale de Lausanne CH-1015 Lausanne Switzerland	1
7.	Mr. G. Derderian Technology Administrator. Airbreathing Propulsion Code AIR-931E Naval Air Systems Command Washington. D.C. 20361	1
8.	Prof. Dr. L. Fottner Institut für Strömungsmaschinen und Strahlantriebe Universität der Bundeswehr München Werner Heisenberg Weg 39 D-8014 Neubiberg Federal Republic of Germany	1
9.	Dr. T. Fransson Department of Aeronautics. Code 67Fr Naval Postgraduate School Monterey. CA 93943-5100	1
10.	Prof. Dr. H. Gallus Institut für Strahlantriebe und Turboarbeitsmaschinen RWTH–Aachen Templergraben 55 D-5100 Aachen Federal Republic of Germany	1

11. Mr. R. Girsberger — 1
Ehrendingerstraße 29
CH-5400 Ennetbaden
Switzerland

12. Dr. G. F. Heiche — 1
Chief Scientist
Code AIR-93D
Naval Air Systems Command
Washington. D.C. 20361

13. Prof. Dr. A. Kluwick — 2
Institut für Strömungslehre und Wärmeübertragung
Technische Universität Wien
Wiedner Hauptstraße 7
A-1040 Wien
Austria

14. Mr. A. Krainer — 10
Department of Aeronautics, Code 67
Naval Postgraduate School
Monterey, CA 93943-5100

15. Dr. A. Moser — 1
Institut für Energietechnik
ETH-Zürich
CH-8092 Zürich
Switzerland

16. Prof. Dr. R. P. Shreeve — 5
Department of Aeronautics, Code 67Sf
Naval Postgraduate School
Monterey, CA 93943-5100

17. Dr. R. J. Simoneau — 1
Chief, Heat Transfer Branch
National Aeronautics and Space Administration
Lewis Research Center
Cleveland, OH 44135

18. Dr. J. M. Verdon — 1
Principal Scientist
United Technologies Research Center
East Hartford, CT 06108

19. Prof. Dr. G. J. Walker — 1
University of Tasmania
GPO Box 252C
Hobart Tasmania 7001
Australia